Table 1 Accumulation levels of ^{99m}Tc-MT1-MMP mAb and ^{99m}Tc-IgG$_3$ in the aortic segments and major organs at 24 h after injection

Segments	^{99m}Tc-MT1-MMP mAb		^{99m}Tc-IgG$_3$
	(a) Control	(b) WHHLMI	(c) WHHLMI
Arch-ascending[a]	0.75±0.37	2.96±1.07**	2.12±0.43***
Thoracic[a]	0.40±0.12	2.48±0.72**	2.03±0.64***
Abdominal[a]	0.27±0.14	1.77±0.50**	0.97±0.51****
Total[a]	0.44±0.29	2.38±0.90**	1.65±0.76****
Blood[a]	3.76±0.89	5.86±0.93*	5.72±1.08
Vastus intermedius muscle[a]	0.23±0.15	0.48±0.64	0.23±0.22
A/B ratio	0.12±0.08	0.40±0.13**	0.30±0.14****
A/M ratio	2.50±1.9	14.3±11.6**	11.0±8.1
Liver[a]	4.23[b]	2.79[b]	ND
Spleen[a]	4.50[b]	3.52[b]	ND
Kidneys[a]	3.79[b]	3.32[b]	ND

Data are represented as the mean ± SD

A/B ratio aorta to blood ratio, *A/M ratio* aorta to muscle ratio, *ND* not determined

*$p<0.05$; **$p<0.001$ vs (a) control group; ***$p<0.05$; ****$p<0.001$ vs (b) ^{99m}Tc-MT1-MMP mAb (WHHLMI) group

[a] DUR

[b] $n=1$ due to technical problems

Accumulation levels of ^{99m}Tc-MT1-MMP mAb in the aortic segments of WHHLMI and control rabbits are summarized in Table 1. The accumulation level in each aortic segment of WHHLMI rabbits was 3.9- to 6.6-fold higher than control rabbits and the differences were significant. Mean blood pool radioactivity at 24 h was 5.86 and 3.76 (DUR) in WHHLMI and control rabbits, respectively. Aorta to blood radioactivity ratios (A/B) and aorta to muscle radioactivity ratios (A/M) were significantly higher in WHHLMI rabbits than in control rabbits. Relatively high ^{99m}Tc-MT1-MMP mAb accumulation levels were detected in the liver (4.23 in WHHLMI and 2.79 in control rabbits), spleen (4.50 in WHHLMI and 3.52 in control rabbits) and kidneys (3.79 in WHHLMI and 3.32 in control rabbits) of both rabbits. No marked difference in the distribution of ^{99m}Tc-MT1-MMP mAb in non-target

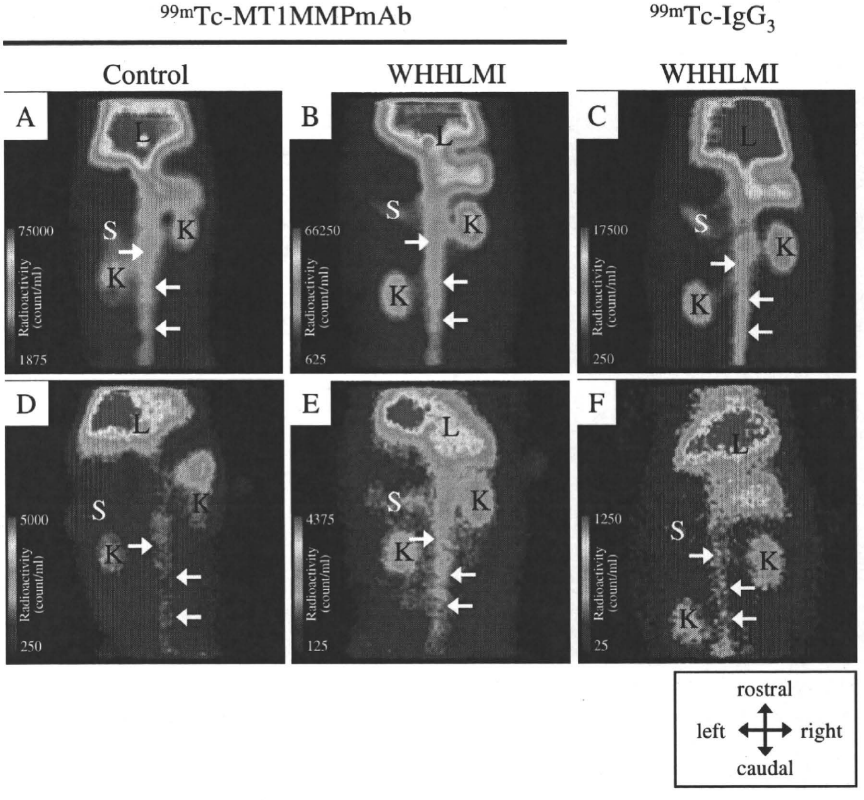

Fig. 3 Non-invasive imaging of the abdominal region with ^{99m}Tc-MT1-MMP mAb and ^{99m}Tc-IgG$_3$. Planar images for the control (**a**, **d**) and WHHLMI rabbits (**b**, **c**, **e**, **f**) at 10 min (**a**–**c**) and 24 h (**d**–**f**) after injection of ^{99m}Tc-MT1-MMP mAb (**a**, **b**, **d**, **e**) or ^{99m}Tc-IgG$_3$ (**c**, **f**). *Arrows*, *L*, *K* and *S* mark the aorta, liver, kidney and spleen, respectively

organs was observed between WHHLMI and control rabbits.

Regional distribution of ^{99m}Tc-MT1-MMP mAb in comparison with MT1-MMP expression

In the ARG study, heterogeneous ^{99m}Tc-MT1-MMP mAb accumulation was observed in the intima of WHHLMI rabbit aortas, while no marked accumulation was found in the aortas of control rabbits (Fig. 4a, b). No marked accumulation was also found in the aortas of WHHLMI rabbits given ^{99m}Tc-IgG$_3$ (Fig. 4c). MT1-MMP expression was detected in the intimal regions of the WHHLMI rabbit aorta, and the expression level was different among the regions (Fig.4e, g, h). Higher accumulation levels of ^{99m}Tc-MT1-MMP mAb were found in regions with high MT1-MMP expression, whereas lower accumulation was observed in regions with low MT1-MMP expression. No obvious MT1-MMP expression was observed in the aorta of control rabbits (Fig. 4d, f). Figure 4i, j shows the relationship of MT1-MMP expression density with ^{99m}Tc-MT1-MMP mAb accumulation and ^{99m}Tc-IgG$_3$, respectively. Regional ^{99m}Tc-MT1-MMP mAb accumulation levels in the aorta section were positively correlated with MT1-MMP expression density in WHHLMI rabbits (r=0.59, p<0.0001). On the other hand, ^{99m}Tc-IgG$_3$ accumulation was independent of MT1-MMP expression density (r=0.03, p=NS).

Relationship between ^{99m}Tc-MT1-MMP mAb accumulation and histological characteristics

Figure 2a–p shows representative photomicrographs of the histological features of each atherosclerotic lesion category in WHHLMI rabbits. The histopathological features, which correspond to the classification criteria, observed in the ascending-arch and thoracic aortas of WHHLMI rabbits were as follows: neointimal (n=15 for ^{99m}Tc-MT1-MMP mAb study and n=13 for ^{99m}Tc-IgG$_3$ study), atheromatous (n=39 and n=31, respectively), fibroatheromatous (n=36 and n=35, respectively) and collagen-rich (n=59 and n=41, respectively). No lesions showed haemorrhage, plaque rupture or thrombi (type VI) in the present study.

^{99m}Tc-MT1-MMP mAb accumulation level was dependent on the histological grade of the lesions (Fig. 5a, Table 2) and was prominently and significantly the highest (p<0.0001) in atheromatous lesions (type IV) compared with those in other lesions. Accumulation level of ^{99m}Tc-MT1-MMP mAb in atheromatous lesions was 3.3-, 2.7- and 3.0-fold higher than those in the neointimal, fibroatheromatous and collagen-rich lesions, respectively. In contrast, the ^{99m}Tc-IgG$_3$ accumulation level was markedly lower than ^{99m}Tc-MT1-MMP mAb. The ^{99m}Tc-IgG$_3$ accumulation level was independent of the histological grade of lesions, except for slightly but significantly lower ^{99m}Tc-IgG$_3$ level in the neointimal lesion (Fig. 5a, Table 2).

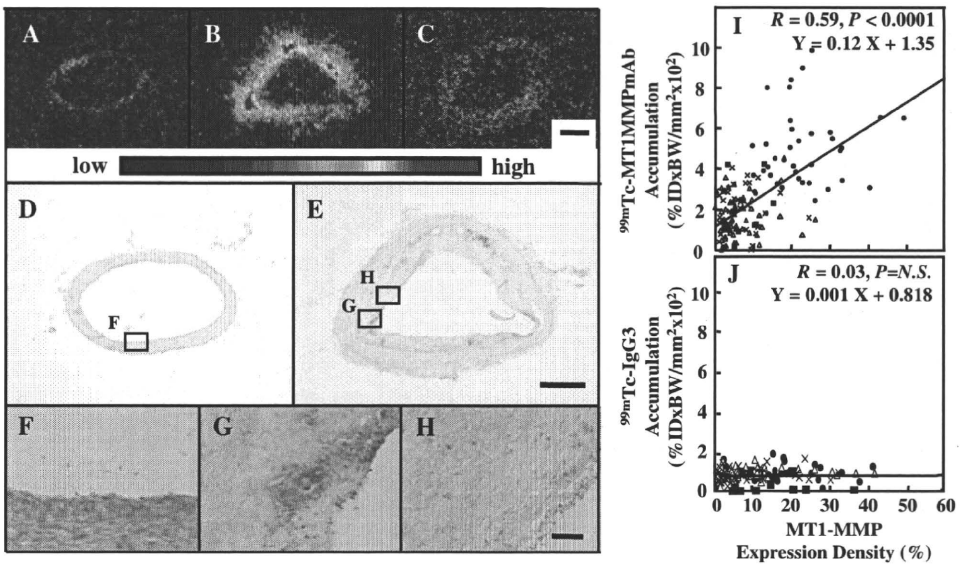

Fig. 4 Regional distribution of ^{99m}Tc-MT1-MMP mAb and ^{99m}Tc-IgG$_3$, and MT1-MMP expression in aorta sections. **a–c** Autoradiograms of ^{99m}Tc-MT1-MMP mAb in the control (**a**) and WHHLMI (**b**) rabbits and ^{99m}Tc-IgG$_3$ in a WHHLMI rabbit (**c**). **d–h** MT1-MMP immunohistochemical staining of the control (**d** and **f**) and WHHLMI rabbits (**e**, **g** and **h**). **f–h** High magnification images of MT1-MMP immunohistochemical staining in the regions depicted in **d** and **e**. Regression analyses of MT1-MMP expression density with ^{99m}Tc-MT1-MMP mAb accumulation (**i**) and ^{99m}Tc-IgG$_3$ (**j**) are shown. An identical colour window was applied to all autoradiographic images (**a–c**). *Bar* = 1 mm (**a–e**) and 100 μm (**f–h**). ■ neointimal lesion, • atheromatous lesion, x fibroatheromatous lesion, Δ collagen-rich lesion

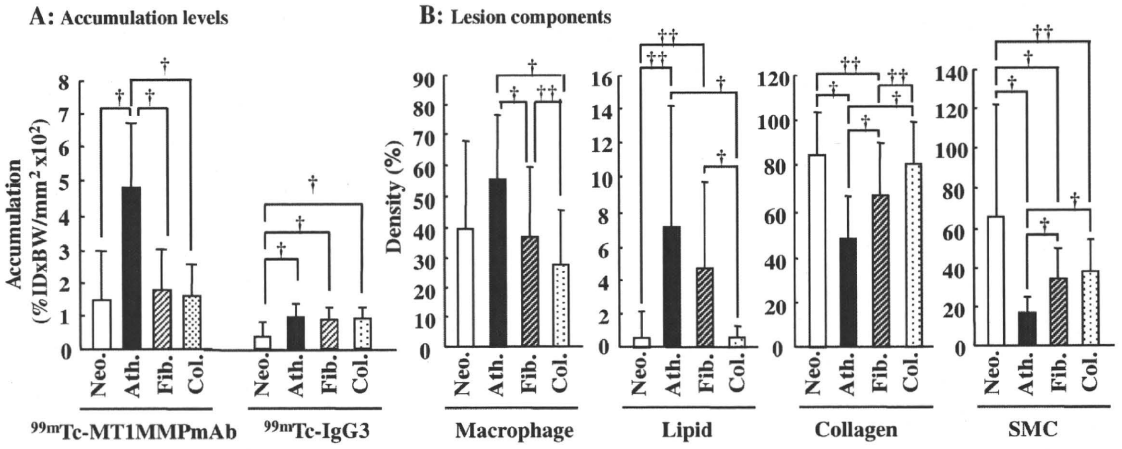

Fig. 5 Distribution profiles of ^{99m}Tc-MT1-MMP mAb, ^{99m}Tc-IgG$_3$ (**a**) and lesion components (macrophages, lipids, collagen and smooth muscle cells) (**b**) in each lesion category. *Neo.*, *Ath.*, *Fib.* and *Col.* neointimal, atheromatous, fibroatheromatous and collagen-rich lesions, respectively. *SMC* smooth muscle cells. Data are represented as the mean ± SD. †$p<0.01$; ††$p<0.05$

Figure 5b and Table 2 show the lesion components (i.e. macrophages, lipids, collagen and smooth muscle cells) quantified for each lesion category. The macrophage and lipid density was also the highest in the atheromatous lesions among the four lesion categories. Consequently, the highest level of ^{99m}Tc-MT1-MMP mAb accumulation, macrophage density and lipid density were observed in atheromatous lesions. On the other hand, the collagen and smooth muscle cell density was the lowest in atheromatous lesions among the four lesion categories.

Discussion

Aiming to develop a non-invasive means for discriminating atherosclerotic lesions at higher risk of rupture (atheromatous lesions) from more stable lesions, the potential of a radio-probe, ^{99m}Tc-MT1-MMP mAb, was evaluated in an atherosclerotic WHHLMI rabbit model. Consequently, significantly higher ^{99m}Tc-MT1-MMP mAb accumulation was found in grade IV atheroma in comparison with neointimal lesions or other more stable lesions. Thus, the potential of ^{99m}Tc-MT1-MMP mAb was demonstrated for nuclear imaging of MT1-MMP expression and selectively detecting atheromatous lesions.

Comparison with ^{99m}Tc-annexin A5 and ^{18}F-FDG

Our major interest is the prominently higher ^{99m}Tc-MT1-MMP mAb accumulation in grade IV atheroma in comparison with neointimal lesions or other more stable lesions. It will be of great importance to compare the accumulation profile of ^{99m}Tc-MT1-MMP mAb with that of ^{99m}Tc-annexin A5, a marker of ongoing apoptotic cell death, and ^{18}F-FDG, a marker of inflammation, as both ^{99m}Tc-annexin A5 and ^{18}F-FDG have been applied to clinical studies and are considered to be the most promising radio-probes for evaluation of plaque characteristics [5, 11]. Surprisingly, the accumulation

Table 2 Distribution profiles of ^{99m}Tc-MT1-MMP mAb, ^{99m}Tc-IgG$_3$ and lesion components (macrophages, lipids, collagen and smooth muscle cells) in each lesion category

	Neointimal	Atheromatous	Fibroatheromatous	Collagen-rich
^{99m}Tc-MT1-MMP mAb[a]	1.48±1.51	4.81±1.91	1.79±1.26	1.60±0.98
^{99m}Tc-IgG$_3$[a]	0.35±0.41	0.93±0.38	0.86±0.32	0.89±0.29
Macrophage[b]	39.8±27.8	55.4±21.3	37.3±22.3	27.8±17.6
Lipid[b]	1.6±2.5	7.2±7.0	4.8±4.9	0.7±0.7
Collagen[b]	84.0±18.9	48.6±18.5	66.9±22.3	80.1±18.3
SMC[b]	65.7±56.5	16.8±8.1	34.4±16.1	38.1±17.2

Data are represented as the mean ± SD. For the results of statistical analysis, see Fig. 5

[a] Accumulation (%ID×BW/mm^2 ×10^2)

[b] Density (%)

ratios of atheromatous lesions to other lesions of ^{99m}Tc-MT1-MMP mAb (**A**theromatous/**N**eointimal = 3.3, **A**theromatous/**F**ibroatheromatous = 2.7 and **A**theromatous/**C**ollagen-rich ratio = 3.0) were markedly higher than those of ^{99m}Tc-annexin A5 (**A/N**=1.3, **A/F**=1.3 and **A/C**=1.8) [28]. These results suggest the ability of ^{99m}Tc-MT1-MMP mAb to selectively detect grade IV atheroma among heterogeneous atherosclerotic lesions. On the other hand, a recent clinical study showed that vascular uptake of FDG was seen in a substantial portion (50%) of patients who had undergone FDG positron emission tomography (PET) imaging for various indications (i.e. malignant tumours, solitary pulmonary nodules or liver masses and benign diseases) [30]. Our previous study in apolipoprotein E null mice also showed relatively high ^{18}F-FDG accumulation levels in early lesions, resulting in lower accumulation ratios for advanced to early lesions in comparison with ^{99m}Tc-annexin A5 [31]. Thus, the desirable features of ^{99m}Tc-MT1-MMP mAb further confirm its potential as a radio-probe for detecting atheromatous lesions. It should be noted here that ^{18}F-FDG is considered to be the most promising probe for identifying inflamed atherosclerotic lesions. This is probably because of the higher absolute uptake levels of ^{18}F-FDG, which may be advantageous for lesion detection [28, 31, 32]. ^{18}F-FDG, as well as CT, MRI and US, can be used to find the patients whose lesion vulnerability needs to be further evaluated. The preferential uptake of ^{99m}Tc-MT1-MMP mAb in atheromatous lesions may be a useful indicator of advanced lesions, although it is still necessary to further demonstrate whether ^{99m}Tc-MT1-MMP mAb is also useful for characterizing atherosclerosis in the course of lesion development, as well as grade IV atheroma.

Immunoreactivity and specificity of ^{99m}Tc-MT1-MMP mAb

Immunoreactivity and specificity are indispensable prerequisites of in vivo nuclear imaging probes utilizing immunodetection. In this study, anti-MT1-MMP monoclonal IgG_3 (MT1-MMP mAb) was labelled with ^{99m}Tc after derivatization with HYNIC. Flow cytometry analyses indicated that modification of MT1-MMP mAb with the chelating moiety (HYNIC) does not significantly affect the immunoreactivity of the original MT1-MMP mAb. In addition, ARG and immunohistochemical studies showed that ^{99m}Tc-MT1-MMP mAb but not ^{99m}Tc-IgG_3 accumulation in atherosclerotic lesions was well correlated with MT1-MMP expression density (Fig. 4i, j). Furthermore, Fig. 5a and Table 2 confirmed the low and almost non-specific accumulation of ^{99m}Tc-IgG_3 among the lesion categories. Our previous studies also showed that accumulation of ^{99m}Tc-labelled non-specific IgG_{2a} in atheromatous lesions was not significantly different from other types of lesions (i.e. neointimal lesion, fibroatheromatous lesion, collagen-rich lesion) [33]. These findings strongly suggest the potential of ^{99m}Tc-MT1-MMP mAb to specifically recognize MT1-MMP in vivo, although experiments using radiotracers with higher radiochemical purities and further characterization of the labelled antibodies are required to confirm the present results and prove the usefulness of nuclear imaging with ^{99m}Tc-MT1-MMP mAb.

Limitations in ^{99m}Tc-MT1-MMP mAb imaging and the present study design

Another prerequisite of radio-probes is a rapid clearance of radioactivity from the blood and tissues surrounding the target lesions. One drawback of our ^{99m}Tc-MT1-MMP mAb is its relatively slow clearance from the blood, which is an intrinsic problem of radio-probes utilizing antibodies. The A/B ratio in WHHLMI rabbits was 0.40±0.13 at 24 h, indicating that the radioactivity detected in the in vivo imaging study was from both the aorta and blood. Thus, the clearance of ^{99m}Tc-MT1-MMP mAb does not match the short half-life of ^{99m}Tc. Recent advances in antibody engineering, however, should provide a promising solution to this issue. Radio-probes derived from low molecular weight polypeptides or compounds, small recombinant antibody fragments (Fab, scFv) or engineered variants (diabodies, triabodies, minibodies and single-domain antibodies) show rapid clearance of radioactivity from the circulation [34]. Pretargeting antibody methods appear to provide another solution to achieve the rapid clearance of radioactivity from the circulation [35]. Image subtraction techniques and/or kinetic model analysis, particularly those with dual isotope single photon emission computed tomography (SPECT) imaging techniques, may also help address this issue [36]. Semiconductor detector technologies contribute to separate signals from each isotope [37]. Accordingly, ^{99m}Tc-MT1-MMP mAb still appears to have the potential as an in vivo nuclear imaging probe that deserves further investigation.

Here, it should be noted that the blood level of ^{99m}Tc-MT1-MMP mAb in WHHLMI rabbits is significantly higher than that in control rabbits (Table 1). Atherosclerotic changes have been shown to be associated with hepatic and renal dysfunctions [38, 39]. Our preliminary in vitro incubation study showed that >95% of ^{99m}Tc-MT1-MMP mAb remained unchanged in rabbit plasma up to 24 h (data not shown). Accordingly, the high blood level of ^{99m}Tc-MT1-MMP mAb in WHHLMI rabbits may be caused by disturbed metabolism/excretion owing to dyshepatia or dysnephria, although the exact reason remains unclear. Our previous study on annexin A5 also showed slower blood clearance of the tracer in WHHLMI rabbits [28].

In addition to the high blood pool radioactivity, the limited spatial resolution of nuclear imaging modalities and cardiac and respiratory motion may hamper imaging of culprit lesions in moving coronary arteries. The limitation, however, may be partly solved by coregistration with CT or MRI to obtain anatomical information [11]. In this regard, PET/CT or SPECT/CT technology has gained increasing interest in the clinical imaging of atherosclerotic plaques. On the other hand, respiratory and electrocardiographic gating techniques seem to be a promising approach to solve the problem of cardiac and respiratory motion [11]. Further, SPECT imaging of small experimental animals is rapidly gaining in popularity, thanks to the development of advanced multi-pinhole collimation technologies [40]. Multi-pinhole collimation technologies may largely improve the spatial resolution of SPECT scanners, although their sensitivity is still limited. Compared with SPECT, PET has several advantages, including its higher resolution with higher sensitivity and better quantitative nature. Accordingly, the development of positron-labelled radiotracers may be another option to solve the limitation, although additional molecular design, including that for accelerating blood clearance and use of positron emitters with longer half-lives (^{64}Cu and ^{124}I), is required.

Hepatic and renal radioactivity accumulation is one of the most important concerns in nuclear imaging utilizing radiolabelled antibodies [41]. The present results showed a relatively high radioactivity accumulation in the kidneys (Table 1). It is well known that most radiolabelled mAbs show very high liver uptake due to the hepatic clearance. Unfortunately, the exact reason for the high renal accumulation remains unclear. However, it may be ascribed to the metabolic and/or degradation products of the labelled compound, as the present experiment performed at 24 h (relatively late phase) after the radiotracer injection. Low molecular weight metabolic and/or degradation products are preferentially excreted via kidneys [41]. Another explanation may be characteristics of the labelled antibody, as ^{99m}Tc-MT1-MMP mAb also showed relatively high renal accumulation in rats and mice at 1 h after the radiotracer injection [42]. Several investigators reported relatively high renal accumulation of radiolabelled mAbs [43–45]. Further studies, including in vivo metabolite analysis, would help clarify the reason for the high renal accumulation of radioactivity derived from ^{99m}Tc-MT1-MMP mAb. On the other hand, the planar images showed significantly higher radioactivity accumulation in the liver than that in the kidneys (Fig. 3). As for the discrepancy between the biodistribution and imaging studies (Table 1 and Fig. 3), the reason can be explained by the planar imaging technique used in the present study. Planar images apparently show higher radioactivity accumulation in the larger (thicker) organs, as they represent summation of radioactivity for the y-axis of the body.

MMPs as a target molecule for imaging plaques at higher risk of rupture

Macrophages secrete enzymes that degrade the fibrous cap of the plaque, including several members of MMPs [16, 46, 47]. MT1-MMP and MMP-2 expression was prominently observed in the macrophage-rich regions of the atheromatous lesions [16]. The high ^{99m}Tc-MT1-MMP mAb accumulation in grade IV atheroma found in the present study can be partly ascribed to the accumulated macrophages in the lesion as shown in Fig. 5 and Table 2. For nuclear imaging of MMPs, several broad-spectrum MMP inhibitors (MPI), including HO-CGS 27023A, have been radiolabelled [11, 12, 48]. Experimental studies in apolipoprotein E null mice indicated that ^{123}I-HO-CGS 27023A could specifically image MMP activity by scintigraphy of MMP-rich vascular lesions in vivo [49]. Another MPI, labelled with ^{111}In (RP780), has been used to image atherosclerotic lesions in a rabbit model [11, 12, 50]. A significantly higher level of immunostaining for MMPs was observed in plaque segments demonstrating higher accumulation of the ^{111}In-labelled MPI. Zhang et al. [51] also showed the potentials of ^{111}In-labelled MPI (RP782), which binds to the activated catalytic domain of MMPs, for detecting injury-induced vascular remodelling in apolipoprotein E null mice. Recently, Fujimoto et al. reported on ^{99m}Tc-labelled MPI (RP805) [52]. On the other hand, Lancelot et al. [53] demonstrated the usefulness of MMPs as a target for the characterization of atherosclerotic lesions, by using a gadolinium (Gd)-based MRI contrast agent that targets MMPs (P947, Gd-labelled MPI). These findings support the present results and indicate the potential of MMPs as a suitable target for in vivo imaging of atherosclerosis. Here, it should be noted that these radiolabelled broad-spectrum MPIs mainly recognize soluble MMPs, including MMP-2, -8, -9 and -13, while our ^{99m}Tc-MT1-MMP mAb recognizes a membrane-bound MMP, MT1-MMP (MMP-14). It may be advantageous to utilize membrane-bound MMPs as a target molecule for imaging because most soluble MMPs are released from cells, which may result in diffuse distribution of the enzymes and elevated circulating MMP levels, and may cause elevated background levels during in vivo imaging. Conversely, it remains unclear and should be clarified which MMP subtype is the most suitable target for in vivo imaging and whether specific or broad-spectrum imaging of MMPs is more useful for determining plaques at higher risk of rupture.

It is very important to discuss the potentials of target molecules other than MMPs. Our previous study in WHHLMI rabbits showed the co-distribution of MT1-

MMP, MMP-2 and cyclooxygenase 2 (COX-2) in grade IV atheroma, indicating a possible link among these enzymes in the destabilization of atherosclerotic plaques [16]. Relatively high COX-2 expression levels, however, were also observed in other more stable lesions, indicating that COX-2 is less suitable for determining plaques at higher risk of rupture. We also evaluated the potentials of lectin-like oxidized low-density lipoprotein (LDL) receptor 1 (LOX-1), a cell surface receptor for oxidized LDL, as a target molecule for determining plaques at higher risk of rupture [33]. Consequently, the accumulation ratios of ^{99m}Tc-labelled anti-LOX-1 mAb for atheromatous lesions to other lesions (**A/N** = 2.7, **A/F** = 1.9 and **A/C** lesion ratios = 2.4) were higher than those of ^{99m}Tc-annexin A5 but less than those of ^{99m}Tc-MT1-MMP mAb. These findings further confirmed the potentials of MT1-MMP as a target molecule for determining plaques at higher risk of rupture. On the other hand, several promising atherosclerosis-targeted imaging agents, including those for macrophage activity, angiogenesis, apoptosis and cell tracking, have been reported [5]. Extensive studies are now ongoing to prove which target molecule is more suitable for characterizing the vulnerability of atherosclerotic plaques and for identifying patients at higher risk of cardiovascular events [5]. Our series of studies in WHHLMI rabbits [28, 33] and apolipoprotein E null mice [31] using ^{18}F-FDG, ^{99m}Tc-annexin A5, ^{99m}Tc-labelled anti-LOX-1 [33] and ^{99m}Tc-MT1-MMP mAb successfully characterized these tracers. Further studies using these animal models should be helpful in the search for a suitable target molecule for imaging atherosclerotic plaques.

Conclusions

In this study, we succeeded in determining MT1-MMP expression in vivo utilizing a radiolabelled anti-MT1-MMP antibody and nuclear imaging techniques. Consequently, we demonstrated prominently higher accumulation of ^{99m}Tc-MT1-MMP mAb in grade IV atheroma. These findings indicate that nuclear imaging of MT1-MMP could provide new diagnostic imaging capabilities for characterizing atherosclerotic plaques, although further investigations to improve the blood clearance and target to blood ratios are strongly required.

Acknowledgments This work was partly supported by a Grant-in-Aid for General Scientific Research from the Ministry of Education, Culture, Sports, Science and Technology of Japan, and from the Japan Society for the Promotion of Science, and by a research grant from New Energy and Industrial Technology Development Organization (NEDO). This study was also partly supported by Special Coordination Funds for Promoting Science and Technology of the Ministry of Education, Culture, Sports, Science and Technology, the Japanese Government.

Conflicts of interest None.

References

1. Kolodgie FD, Virmani R, Burke AP, Farb A, Weber DK, Kutys R, et al. Pathologic assessment of the vulnerable human coronary plaque. Heart 2004;90:1385–91.
2. Lendon C, Born GV, Davies MJ, Richardson PD. Plaque fissure: the link between atherosclerosis and thrombosis. Nouv Rev Fr Hematol 1992;34:27–9.
3. Ruberg FL, Leopold JA, Loscalzo J. Atherothrombosis: plaque instability and thrombogenesis. Prog Cardiovasc Dis 2002;44:381–94.
4. Davies JR, Rudd JH, Weissberg PL. Molecular and metabolic imaging of atherosclerosis. J Nucl Med 2004;45:1898–907.
5. Jaffer FA, Libby P, Weissleder R. Molecular and cellular imaging of atherosclerosis: emerging applications. J Am Coll Cardiol 2006;47:1328–38.
6. Galis ZS, Khatri JJ. Matrix metalloproteinases in vascular remodeling and atherogenesis: the good, the bad, and the ugly. Circ Res 2002;90:251–62.
7. Galis ZS, Sukhova GK, Lark MW, Libby P. Increased expression of matrix metalloproteinases and matrix degrading activity in vulnerable regions of human atherosclerotic plaques. J Clin Invest 1994;94:2493–503.
8. Jones CB, Sane DC, Herrington DM. Matrix metalloproteinases: a review of their structure and role in acute coronary syndrome. Cardiovasc Res 2003;59:812–23.
9. Brown DL, Hibbs MS, Kearney M, Loushin C, Isner JM. Identification of 92-kD gelatinase in human coronary atherosclerotic lesions. Association of active enzyme synthesis with unstable angina. Circulation 1995;91:2125–31.
10. Li Z, Li L, Zielke HR, Cheng L, Xiao R, Crow MT, et al. Increased expression of 72-kd type IV collagenase (MMP-2) in human aortic atherosclerotic lesions. Am J Pathol 1996;148:121–8.
11. Davies JR, Rudd JH, Weissberg PL, Narula J. Radionuclide imaging for the detection of inflammation in vulnerable plaques. J Am Coll Cardiol 2006;47:C57–68.
12. Hartung D, Schäfers M, Fujimoto S, Levkau B, Narula N, Kopka K, et al. Targeting of matrix metalloproteinase activation for noninvasive detection of vulnerable atherosclerotic lesions. Eur J Nucl Med Mol Imaging 2007;34:S1–8.
13. Visse R, Nagase H. Matrix metalloproteinases and tissue inhibitors of metalloproteinases: structure, function, and biochemistry. Circ Res 2003;92:827–39.
14. Sato H, Takino T, Okada Y, Cao J, Shinagawa A, Yamamoto E, et al. A matrix metalloproteinase expressed on the surface of invasive tumour cells. Nature 1994;370:61–5.
15. Knäuper V, Bailey L, Worley JR, Soloway P, Patterson ML, Murphy G. Cellular activation of proMMP-13 by MT1-MMP depends on the C-terminal domain of MMP-13. FEBS Lett 2002;532:127–30.
16. Kuge Y, Takai N, Ishino S, Temma T, Shiomi M, Saji H. Distribution profiles of membrane type-1 matrix metalloproteinase (MT1-MMP), matrix metalloproteinase-2 (MMP-2) and cyclooxygenase-2 (COX-2) in rabbit atherosclerosis: comparison with plaque instability analysis. Biol Pharm Bull 2007;30:1634–40.
17. Rajavashisth TB, Xu XP, Jovinge S, Meisel S, Xu XO, Chai NN, et al. Membrane type 1 matrix metalloproteinase expression in human atherosclerotic plaques: evidence for activation by proinflammatory mediators. Circulation 1999;99:3103–9.
18. Stawowy P, Meyborg H, Stibenz D, Borges Pereira Stawowy N, Roser M, Thanabalasingam U, et al. Furin-like proprotein convertases are central regulators of the membrane type matrix

metalloproteinase-pro-matrix metalloproteinase-2 proteolytic cascade in atherosclerosis. Circulation 2005;111:2820–7.
19. Shiomi M, Ito T, Yamada S, Kawashima S, Fan J. Development of an animal model for spontaneous myocardial infarction (WHHLMI rabbit). Arterioscler Thromb Vasc Biol 2003;23:1239–44.
20. Abrams MJ, Juweid M, tenKate CI, Schwartz DA, Hauser MM, Gaul FE, et al. Technetium-99m-human polyclonal IgG radiolabeled via the hydrazino nicotinamide derivative for imaging focal sites of infection in rats. J Nucl Med 1990;31:2022–8.
21. Ono M, Arano Y, Mukai T, Uehara T, Fujioka Y, Ogawa K, et al. Plasma protein binding of (99m)Tc-labeled hydrazino nicotinamide derivatized polypeptides and peptides. Nucl Med Biol 2001;28:155–64.
22. Ono M, Arano Y, Uehara T, Yasushi F, Kazuma O, Namba S, et al. Intracellular metabolic fate of radioactivity after injection of technetium-99m-labeled hydrazino nicotinamide derivatized proteins. Bioconjug Chem 1999;10:386–94.
23. Larsen SK, Solomon HF, Caldwell G, Abrams MJ. [99mTc]tricine: a useful precursor complex for the radiolabeling of hydrazinonicotinate protein conjugates. Bioconjug Chem 1995;6:635–8.
24. Ishii K, Kita T, Kume N, Nagano Y, Kawai C. Uptake of acetylated LDL by peritoneal macrophages obtained from normal and Watanabe heritable hyperlipidemic rabbits, an animal model for familial hypercholesterolemia. Biochim Biophys Acta 1988;962:387–9.
25. Stary HC, Chandler AB, Dinsmore RE, Fuster V, Glagov S, Insull Jr W, et al. A definition of advanced types of atherosclerotic lesions and a histological classification of atherosclerosis. A report from the Committee on Vascular Lesions of the Council on Arteriosclerosis, American Heart Association. Circulation 1995;92:1355–74.
26. Stary HC, Chandler AB, Glagov S, Guyton JR, Insull Jr W, Rosenfeld ME, et al. A definition of initial, fatty streak, and intermediate lesions of atherosclerosis. A report from the Committee on Vascular Lesions of the Council on Arteriosclerosis, American Heart Association. Circulation 1994;89:2462–78.
27. Kobayashi S, Inoue N, Ohashi Y, Terashima M, Matsui K, Mori T, et al. Interaction of oxidative stress and inflammatory response in coronary plaque instability: important role of C-reactive protein. Arterioscler Thromb Vasc Biol 2003;23:1398–404.
28. Ishino S, Kuge Y, Takai N, Tamaki N, Strauss HW, Blankenberg FG, et al. 99mTc-Annexin A5 for noninvasive characterization of atherosclerotic lesions: imaging and histological studies in myocardial infarction-prone Watanabe heritable hyperlipidemic rabbits. Eur J Nucl Med Mol Imaging 2007;34:889–99.
29. Shiomi M, Ito T, Hirouchi Y, Enomoto M. Stability of atheromatous plaque affected by lesional composition: study of WHHL rabbits treated with statins. Ann N Y Acad Sci 2001;947:419–23.
30. Yun M, Yeh D, Araujo LI, Jang S, Newberg A, Alavi A. F-18 FDG uptake in the large arteries: a new observation. Clin Nucl Med 2001;26:314–9.
31. Zhao Y, Kuge Y, Zhao S, Morita K, Inubushi M, Strauss HW, et al. Comparison of 99mTc-annexin A5 with 18F-FDG for the detection of atherosclerosis in ApoE-/- mice. Eur J Nucl Med Mol Imaging 2007;34:1747–55.
32. Ogawa M, Ishino S, Mukai T, Asano D, Teramoto N, Watabe H, et al. (18)F-FDG accumulation in atherosclerotic plaques: immunohistochemical and PET imaging study. J Nucl Med 2004;45:1245–50.
33. Ishino S, Mukai T, Kuge Y, Kume N, Ogawa M, Takai N, et al. Targeting of lectinlike oxidized low-density lipoprotein receptor 1 (LOX-1) with 99mTc-labeled anti-LOX-1 antibody: a potential agent for imaging of vulnerable plaque. J Nucl Med 2008;49:1677–85.
34. Huhalov A, Chester KA. Engineered single chain antibody fragments for radioimmunotherapy. Q J Nucl Med Mol Imaging 2004;48:279–88.
35. Sharkey RM, Karacay H, Cardillo TM, Chang CH, McBride WJ, Rossi EA, et al. Improving the delivery of radionuclides for imaging and therapy of cancer using pretargeting methods. Clin Cancer Res 2005;11:7109s–21.
36. Watabe H, Ikoma Y, Kimura Y, Naganawa M, Shidahara M. PET kinetic analysis–compartmental model. Ann Nucl Med 2006;20:583–8.
37. Darambara DG, Todd-Pokropek A. Solid state detectors in nuclear medicine. Q J Nucl Med 2002;46:3–7.
38. Campean V, Neureiter D, Varga I, Runk F, Reiman A, Garlichs C, et al. Atherosclerosis and vascular calcification in chronic renal failure. Kidney Blood Press Res 2005;28:280–9.
39. Santoliquido A, Di Campli C, Miele L, Gabrieli ML, Forgione A, Zocco MA, et al. Hepatic steatosis and vascular disease. Eur Rev Med Pharmacol Sci 2005;9:269–71.
40. Beekman F, van der Have F. The pinhole: gateway to ultra-high-resolution three-dimensional radionuclide imaging. Eur J Nucl Med Mol Imaging 2007;34:151–61.
41. Akizawa H, Arano Y. Altering pharmacokinetics of radiolabeled antibodies by the interposition of metabolizable linkages. Metabolizable linkers and pharmacokinetics of monoclonal antibodies. Q J Nucl Med 2002;46:206–23.
42. Temma T, Sano K, Kuge Y, Kamihashi J, Takai N, Ogawa Y, et al. Development of a radiolabeled probe for detecting membrane type-1 matrix metalloproteinase on malignant tumors. Biol Pharm Bull 2009;32:1272–7.
43. Rogers BE, Anderson CJ, Connett JM, Guo LW, Edwards WB, Sherman EL, et al. Comparison of four bifunctional chelates for radiolabeling monoclonal antibodies with copper radioisotopes: biodistribution and metabolism. Bioconjug Chem 1996;7:511–22.
44. Sugimoto K, Nishimoto N, Kishimoto T, Yoshizaki K, Nishimura T. Imaging of lesions in a murine rheumatoid arthritis model with a humanized anti-interleukin-6 receptor antibody. Ann Nucl Med 2005;19:261–6.
45. D'Alessandria C, Malviya G, Viscido A, Aratari A, Maccioni F, Amato A, et al. Use of a 99mTc labeled anti-TNFalpha monoclonal antibody in Crohn's disease: in vitro and in vivo studies. Q J Nucl Med Mol Imaging 2007;51:334–42.
46. Cipollone F, Fazia M, Mezzetti A. Novel determinants of plaque instability. J Thromb Haemost 2005;3:1962–75.
47. Rudd JH, Hyafil F, Fayad ZA. Inflammation imaging in atherosclerosis. Arterioscler Thromb Vasc Biol 2009;29:1009–16.
48. Breyholz HJ, Wagner S, Levkau B, Schober O, Schäfers M, Kopka K. A 18F-radiolabeled analogue of CGS 27023A as a potential agent for assessment of matrix-metalloproteinase activity in vivo. Q J Nucl Med Mol Imaging 2007;51:24–32.
49. Schäfers M, Riemann B, Kopka K, Breyholz HJ, Wagner S, Schäfers KP, et al. Scintigraphic imaging of matrix metalloproteinase activity in the arterial wall in vivo. Circulation 2004;109: 2554–9.
50. Kolodgie F, Edwards S, Petrov A, Sachleben R, Hartung D, Weber DK. Noninvasive detection of matrix metalloproteinase upregulation in experimental atherosclerotic lesions and its abrogation by dietary modification [abstract]. Circulation 2001; 104:694.
51. Zhang J, Nie L, Razavian M, Ahmed M, Dobrucki LW, Asadi A, et al. Molecular imaging of activated matrix metalloproteinases in vascular remodeling. Circulation 2008;118:1953–60.
52. Fujimoto S, Hartung D, Ohshima S, Edwards DS, Zhou J, Yalamanchili P, et al. Molecular imaging of matrix metalloproteinase in atherosclerotic lesions: resolution with dietary modification and statin therapy. J Am Coll Cardiol 2008;52:1847–57.
53. Lancelot E, Amirbekian V, Brigger I, Raynaud JS, Ballet S, David C, et al. Evaluation of matrix metalloproteinases in atherosclerosis using a novel noninvasive imaging approach. Arterioscler Thromb Vasc Biol 2008;28:425–32.

Tissue Factor Detection for Selectively Discriminating Unstable Plaques in an Atherosclerotic Rabbit Model

Takashi Temma[1], Yuki Ogawa[1], Yuji Kuge[1,2], Seigo Ishino[1], Nozomi Takai[1], Kantaro Nishigori[1], Masashi Shiomi[3], Masahiro Ono[1], and Hideo Saji[1]

[1]Department of Patho-Functional Bioanalysis, Graduate School of Pharmaceutical Sciences, Kyoto University, Sakyo-ku, Kyoto, Japan; [2]Central Institute of Isotope Science, Hokkaido University, Kita-ku, Sapporo, Japan; and [3]Institute for Experimental Animals, Kobe University Graduate School of Medicine, Chuo-ku, Kobe, Japan

Tissue factor (TF), a transmembrane glycoprotein that acts as an essential cofactor to factor VII/VIIa, initiates the exogenous blood coagulation cascade leading to thrombin generation and subsequent thrombus formation in vivo. TF expression is closely related to plaque vulnerability, and high TF expression is shown in macrophage-rich atheromatous lesions, making TF a potential target for detecting atheromatous lesions in vivo. Thus, we prepared ^{99m}Tc-labeled anti-TF-monoclonal antibody (TF-mAb) IgG as a molecular probe and evaluated its usefulness to achieve TF-specific imaging using myocardial infarction–prone Watanabe heritable hyperlipidemic (WHHLMI) rabbits. **Methods:** Anti-TF-mAb was created using a standard hybridoma technique and was labeled by ^{99m}Tc with 6-hydrazinonicotinic acid (HYNIC) as a chelating agent to obtain ^{99m}Tc-TF-mAb. The immunoreactivity of HYNIC-TF-mAb was estimated by flow cytometry. WHHLMI and control rabbits were injected intravenously with ^{99m}Tc-TF-mAb. Twenty-four hours after the injection, the aorta was removed and radioactivity was measured. Autoradiography and histologic studies were performed using serial aorta sections. Subclass matched antibody (IgG_1) was used as a negative control. **Results:** HYNIC-TF-mAb showed 93% immunoreactivity of the anti-TF-mAb. The radioactivity accumulation in WHHLMI aortas was 6.1-fold higher than that of control rabbits. Autoradiograms showed a heterogeneous distribution of radioactivity in the intima of WHHLMI aortas. Regional radioactivity accumulation was positively correlated with TF expression density ($R = 0.64$, $P < 0.0001$). The highest radioactivity accumulation in percentage injected dose × body weight/mm^2 × 10^2 was found in atheromatous lesions (5.2 ± 1.9) followed by fibroatheromatous (2.1 ± 0.7), collagen-rich (1.8 ± 0.7), and neointimal lesions (1.8 ± 0.6). In contrast, ^{99m}Tc-IgG_1 showed low radioactivity accumulation in WHHLMI aortas that was independent of the histologic grade of lesions. **Conclusion:** The TF-detecting ability and preferential accumulation in atheromatous lesions of ^{99m}Tc-TF-mAb were demonstrated, indicating its potential for selective imaging of macrophage-rich atheromatous lesions in vivo.

Key Words: tissue factor; radioimmunodetection; thrombus; atherosclerotic plaque

J Nucl Med 2010; 51:1979–1986
DOI: 10.2967/jnumed.110.081216

Thrombus formation triggered by plaque rupture is the most important mechanism leading to the onset of acute arterial disease and ischemic sudden death. Thus, the development of a method for detecting thrombus-forming vulnerable plaques before rupture has been clinically desired to more precisely estimate risk and provide effective treatment. Although several molecular imaging probes have been investigated (*1,2*), the target molecules of such probes were not directly related to the thrombotic process.

Tissue factor (TF), a transmembrane glycoprotein that acts as an essential cofactor to factor (F) VII/VIIa, initiates the exogenous blood coagulation cascade leading to thrombin generation and subsequent thrombus formation. TF expression was identified in atherosclerotic lesions, including in endothelial cells, smooth muscle cells, monocytes, and, especially, macrophages or foam cells (*3*). In human pathologic lesions, the TF content of de novo lipid-rich plaques was higher than that of stenotic fibrous plaques (*4*), and such lipid-rich plaque tissue was 6 times more thrombogenic than fibrous plaques. In addition, our recent study also demonstrated that TF expression was closely related to plaque vulnerability, with high TF expression specifically in macrophage-rich atheromatous lesions among heterogeneous atherosclerotic lesions (*5*). Given these data, TF is a potential target for probes detecting atheromatous lesions at higher risk for rupture in vivo.

In the present study, we prepared a monoclonal antibody to TF (TF-mAb) and labeled it with ^{99m}Tc (^{99m}Tc-TF-mAb) as a molecular probe. Using an atherosclerosis model (myocardial infarction–prone Watanabe heritable hyperlipidemic [WHHLMI] rabbits) (*6*), we investigated the accumulation of ^{99m}Tc-TF-mAb in atherosclerotic lesions in comparison with histologic characteristics and evaluated the potential of ^{99m}Tc-TF-mAb as a molecular probe for detecting vulnerable atheromatous lesions.

Received Jul. 13, 2010; revision accepted Sep. 8, 2010.
For correspondence or reprints contact: Yuji Kuge, Central Institute of Isotope Science, Hokkaido University, Kita 15 Nishi 7, Kita-ku, Sapporo 060-8638, Japan.
E-mail: kuge@ric.hokudai.ac.jp

MATERIALS AND METHODS

Design and Preparation of ^{99m}Tc-TF-mAb and ^{99m}Tc-IgG$_1$

A monoclonal antibody (mouse IgG$_1$ subclass) for rabbit TF (193Ser-207Cys, extracellular domain) was established using a standard hybridoma technique. ^{99m}Tc-pertechnetate was eluted in saline solution on a daily basis from ^{99}Mo–^{99m}Tc generators (Ultra-Techne Kow; FUJIFILM RI Pharma Co., Ltd.).

Anti-TF-mAb was radiolabeled with ^{99m}Tc (^{99m}Tc-TF-mAb) after derivatization with 6-hydrazinonicotinic acid (HYNIC) (*7*), as previously reported (*8*). In brief, HYNIC-*N*-hydroxysuccinimide was reacted with TF-mAb, and the mixture was purified by size-exclusion filtration with a diafiltration membrane (Amicon Ultra 4 [molecular weight cutoff, 30,000]; Millipore Co.). An equal volume of ^{99m}Tc-(tricine)$_2$, prepared by the method of Larsen et al. (*9*), was added to the purified solution of HYNIC-TF-mAb to obtain ^{99m}Tc-TF-mAb. After purification by size-exclusion filtration with a PD-10 column, the radiochemical purity of ^{99m}Tc-TF-mAb was more than 95% by another size-exclusion filtration.

For the control study, negative control mouse IgG$_1$ (0102-01; Southern Biotechnology Associates Inc.) was used for the preparation of ^{99m}Tc-IgG$_1$. The radiochemical purity of ^{99m}Tc-IgG$_1$ was also estimated to be more than 95%.

Animals

All animal procedures were approved by the Kyoto University Animal Care Committee. Three male Japanese White rabbits (age, 3 mo) were used to obtain peritoneal macrophages. For biodistribution studies of ^{99m}Tc-TF-mAb, 5 WHHLMI rabbits (4 male, 1 female; age, 12–18 mo; mean weight ± SD, 3.4 ± 0.2 kg; supplied by the Institute for Experimental Animals, Kobe University School of Medicine, Japan) were used. Four male Japanese White rabbits (age, 3 mo; mean weight ± SD, 1.9 ± 0.2 kg) were used for the control study. For ^{99m}Tc-IgG$_1$ studies, 3 WHHLMI rabbits (1 male and 2 female; age, 11–12 mo; mean weight ± SD, 3.2 ± 0.1 kg) were used. The animals were fed standard chow and given water ad libitum.

Immunoreactivity of HYNIC-TF-mAb

Rabbit peritoneal macrophages were obtained by the method of Ishii et al. (*10*), with minor modifications. Cells were suspended at a final concentration of 2.5×10^6 cells/mL in medium A (Dulbecco's modified Eagle's medium containing 1 mM glutamine, 100 U of penicillin per milliliter, 100 mg of streptomycin per milliliter [pH 7.4], and 0.2% lactalbumin hydrolysate). Aliquots of the cell suspension were cultured in plastic petri dishes in a humidified 5% CO_2 incubator at 37°C. After 2 h, each dish was washed twice with 10 mL of medium A to remove nonadherent cells. Monolayers were cultured for 18 h at 37°C in 20 mL of medium A, and cells were washed twice with 10 mL of medium A and then used for experiments. More than 95% of the cells were viable, as determined by a trypan blue exclusion test, and almost all of the attached cells showed positive nonspecific esterase staining.

Antibodies (5 μg/mL, 100 μL; TF-mAb, HYNIC-TF-mAb, or negative control IgG$_1$) were added to the cells (10^6) and incubated for 30 min at 4°C. After cells were washed, Alexa Fluor 488 goat antimouse IgG antibody (x0931; DakoCytomation) (10 μg/mL, 100 μL) was added for 30 min at 4°C. Fluorescence levels were measured using a flow cytometer (Becton Dickinson Inc.). Data were analyzed using BD CellQuest Pro (BD Biosciences), and an immunoreactivity index was calculated as the ratio of the median fluorescence intensity for either TF-mAb or HYNIC-TF-mAb to that of negative-control IgG$_1$. Measurements were performed 3 times per rabbit using 3 Japanese White rabbits, and the ratios were expressed as mean ± SD.

Biodistribution Studies

A simple schematic of our experimental protocol is shown in Figure 1. After 12 h of fasting, rabbits were initially anesthetized with ketamine (intramuscularly, 35 mg/kg) and xylazine (intramuscularly, 5 mg/kg). Either ^{99m}Tc-TF-mAb (547–1,024 MBq,

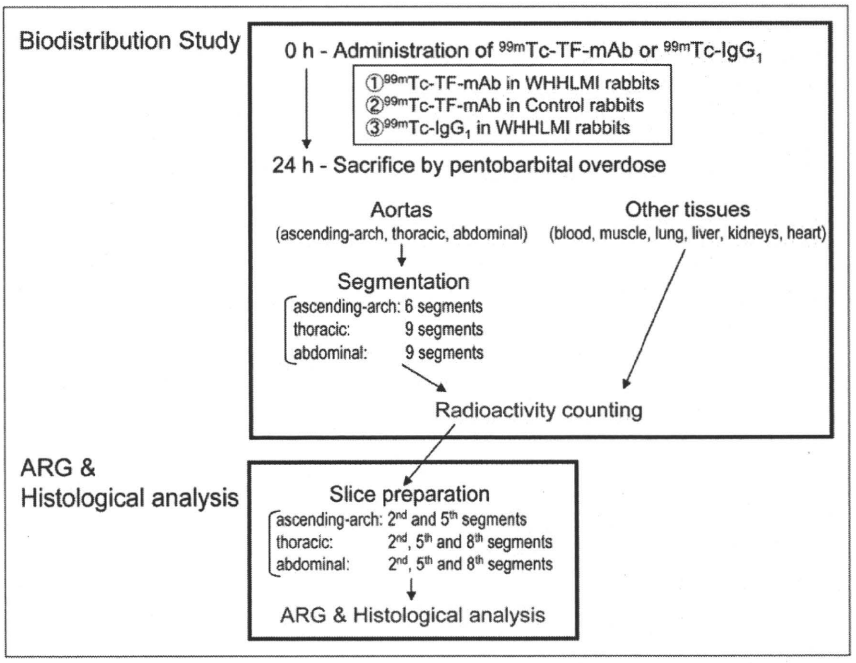

FIGURE 1. Simple schematic of this study. ARG = autoradiography.

300 μg) or ^{99m}Tc-IgG$_1$ (848–1,038 MBq, 300 μg) was injected into a marginal ear vein (5 WHHLMI rabbits and 4 control rabbits for the ^{99m}Tc-TF-mAb study, 3 WHHLMI rabbits for the ^{99m}Tc-IgG$_1$ study). Twenty-four hours after the injection, animals were sacrificed by pentobarbital overdose. The ascending-arch, thoracic, and abdominal aortas, blood, and other tissues (muscle, lung, liver, kidneys, and heart) were removed. The ascending-arch aortas were divided into 6 segments, and the thoracic and abdominal aortas were divided into 9 segments. Each segment was weighed and immediately fixed in a solution containing L-(+)-lysine hydrochloride (75 mM) and 4% paraformaldehyde in phosphate buffer (37.5 mM, pH 7.4) (*11*). The radioactivity of each sample was measured with a well-type γ-counter (1480 Wizard 3″; PerkinElmer Japan Co.). The results were expressed as the differential uptake ratio (DUR), calculated as (tissue activity/tissue weight)/(injected radiotracer activity/animal body weight), with activities given in becquerels and weights in grams. The aorta-to-blood (A/B) ratio and the aorta-to-muscle (A/M) ratio were calculated from the DUR for each tissue sample.

Autoradiography

Eight segments, the second and fifth segments of the ascending aortic arch and the second, fifth, and eighth segments from the thoracic and the abdominal aortas, from each animal were used for autoradiography studies. These segments were frozen and cut into 20-μm-thick slices with a cryomicrotome. The sections were thawed and mounted on silane-coated slides, which were then placed on a phosphor image plate (Fuji Imaging Plate BAS-MS; Fuji Photo Film) for 24 h together with a calibrated standard ($^{99m}TcO_4^-$ solution). The autoradiography images were analyzed with a computerized imaging analysis system (Bio Imaging Analyzer BAS2500 and Image Gauge Software; Fuji Photo Film). The radioactivity in each region of interest was expressed as percentage injected dose × body weight/mm^2, calculated as (radioactivity in the region of interest)/(injected radioactivity/animal body weight).

Histologic Analysis

The tissue sections used for autoradiography studies were also subjected to Azan–Mallory and hematoxylin and eosin staining. Serial sections of the slices from the autoradiography studies were subjected to immunohistochemical staining (for TF, macrophages, and smooth muscle cells) using specific antibodies and an Envision+ kit (Dako) with hematoxylin counterstaining. The antibodies used were TF-mAb (4510; American Diagnostica Inc.), rabbit macrophage–specific mAb RAM-11 (Dako), and human smooth-muscle actin–specific mAb 1A4 (Dako). Immunostaining with subclass-matched irrelevant IgG served as a negative control. Azan–Mallory and hematoxylin and eosin staining were performed by standard procedures. TF expression density was determined as a percentage of the positively stained region using a VHX digital microscope (Keyence Corp.).

Classification of Atherosclerotic Lesions

We divided atherosclerotic lesions in WHHLMI rabbits into the following 4 categories, using a classification scheme based on the recommendations of the American Heart Association (*12,13*) and Azan–Mallory and hematoxylin and eosin staining, as previously described (*14–17*): neointimal (types I–III), atheromatous (type IV), fibroatheromatous (types Va and Vb), and collagen-rich (type Vc). Supplemental Figures 1A–1P (supplemental materials are available online only at http://jnm.snmjournals.org) show representative photomicrographs of the histologic features of each atherosclerotic lesion category in WHHLMI rabbits.

Regions of interest were placed to cover each atherosclerotic lesion in the aortic section of the WHHLMI rabbit and then transferred to the corresponding autoradiography images (Supplemental Figs. 1Q–1S).

Vulnerability Index

An index of morphologic destabilization characteristics, the vulnerability index, was calculated for each lesion in the WHHLMI rabbits by the method of Shiomi et al. (*18*). The vulnerability index was defined as the ratio of the lipid component area (macrophages and extracellular lipid deposits) to the fibromuscular component area (smooth muscle cells and collagen fibers). Collagen fibers and extracellular lipid deposits (extracellular vacuoles and lacunae) were determined with Azan–Mallory stain-

TABLE 1
Accumulation Levels of ^{99m}Tc-TF-mAb and ^{99m}Tc-IgG$_1$ in Aortic Segments of Control and WHHLMI Rabbits at 24 Hours After Injection

Segments	^{99m}Tc-TF-mAb		^{99m}Tc-IgG$_1$, WHHLMI
	Control	WHHLMI	
Ascending arch	0.60 ± 0.05	3.08 ± 0.57*†	2.05 ± 0.42*
Thoracic	0.51 ± 0.11	3.07 ± 1.44*‡	1.60 ± 0.44*
Abdominal	0.35 ± 0.06	2.49 ± 0.64*‡	0.76 ± 0.16*
Total	0.47 ± 0.04	2.86 ± 0.85*‡	1.40 ± 0.24*
Blood	4.0 ± 0.6	7.5 ± 0.0*	7.1 ± 0.7§
Femoral muscle	0.6 ± 0.5	0.3 ± 0.2	0.4 ± 0.1
Aorta-to-blood ratio	0.12 ± 0.02	0.38 ± 0.09*‡	0.20 ± 0.02*
Aorta-to-muscle ratio	1.0 ± 0.6	19.3 ± 19.1*‡	4.0 ± 0.4*

*$P < 0.0001$ vs. control rabbits in ^{99m}Tc-TF-mAb study.
†$P < 0.001$ vs. WHHLMI rabbits in ^{99m}Tc-IgG$_1$ study.
‡$P < 0.0001$ vs. WHHLMI rabbits in ^{99m}Tc-IgG$_1$ study.
§$P < 0.001$, vs. control rabbits in ^{99m}Tc-TF-mAb study.
Data are represented as mean ± SD of DUR.

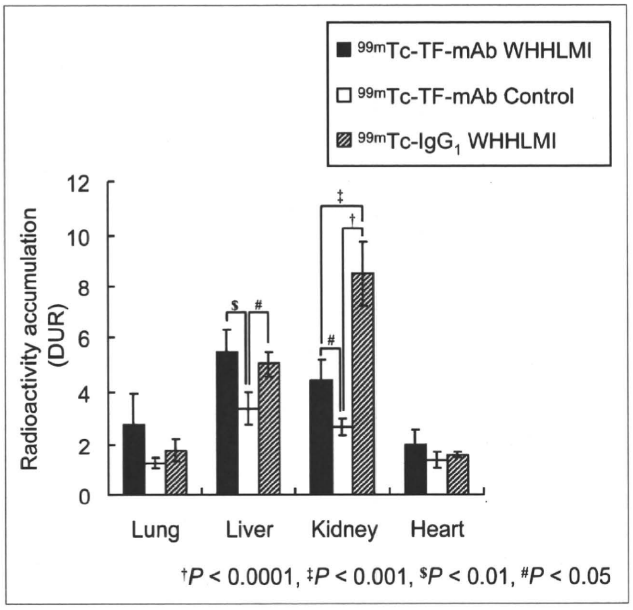

FIGURE 2. Radioactivity distribution in lung, liver, kidneys, and heart. Data are mean ± SD. †$P < 0.0001$. ‡$P < 0.001$. $$P < 0.01$. #$P < 0.05$.

ing. Macrophages and smooth muscle cells were determined with immunohistochemical staining (*17*).

Statistical Analysis

Data are presented as mean ± SD. Statistical analysis was performed with the Mann–Whitney *U* test to compare aortic segments of WHHLMI and control rabbits (Table 1). Radioactivity that accumulated in nontargeted organs among antibodies and animals was compared using 1-way ANOVA, with post hoc analysis by the Holm test (Fig. 2). Correlation coefficients were assessed by Spearman rank correlation coefficients (Fig. 3). Lesion types were compared using the Kruskal–Wallis test, with post hoc analysis by the Scheffé test (Fig. 4). A 2-tailed value of *P* less than 0.05 was considered statistically significant.

RESULTS

Immunoreactivity of HYNIC-TF-mAb

Using fluorescent-activated cell sorter analysis of rabbit peritoneal macrophages, we could clearly distinguish the signals of TF-mAb and HYNIC-TF-mAb from that of the negative control IgG_1. The median fluorescence intensity ratios of TF-mAb and HYNIC-TF-mAb to control IgG_1 were 2.90 ± 0.06 and 2.69 ± 0.11, respectively, and the difference between the labeled and unlabeled TF antibodies was not statistically significant.

Biodistribution Studies

Accumulation levels of ^{99m}Tc-TF-mAb and ^{99m}Tc-IgG_1 in the aortic segments of WHHLMI and control rabbits are summarized in Table 1. The accumulation level of ^{99m}Tc-TF-mAb in each aortic segment of WHHLMI rabbits (ascending arch, 3.08 ± 0.57 DUR; thoracic, 3.07 ± 1.44 DUR; and abdominal, 2.49 ± 0.64 DUR) was 5.1- to 7.1-fold higher than that of control rabbits (ascending arch, 0.60 ± 0.05 DUR; thoracic, 0.51 ± 0.11 DUR; and abdominal, 0.35 ± 0.06 DUR), and the differences were significant in each case. Blood-pool radioactivity levels of ^{99m}Tc-TF-mAb at 24 h were 7.5 ± 0.0 and 4.0 ± 0.6 DUR in WHHLMI and control rabbits, respectively. A/B and A/M ratios were significantly higher in WHHLMI rabbits than in control rabbits (A/B, 0.38 ± 0.09 in WHHLMI and 0.12 ± 0.02 in control rabbits; A/M, 19.3 ± 19.1 in WHHLMI and 1.0 ± 0.6 in control rabbits). In addition, the level of ^{99m}Tc-TF-mAb accumulation in WHHLMI rabbit aortas was 1.5- to 3.3-fold higher than the level of ^{99m}Tc-IgG_1 accumulation, and the differences were significant.

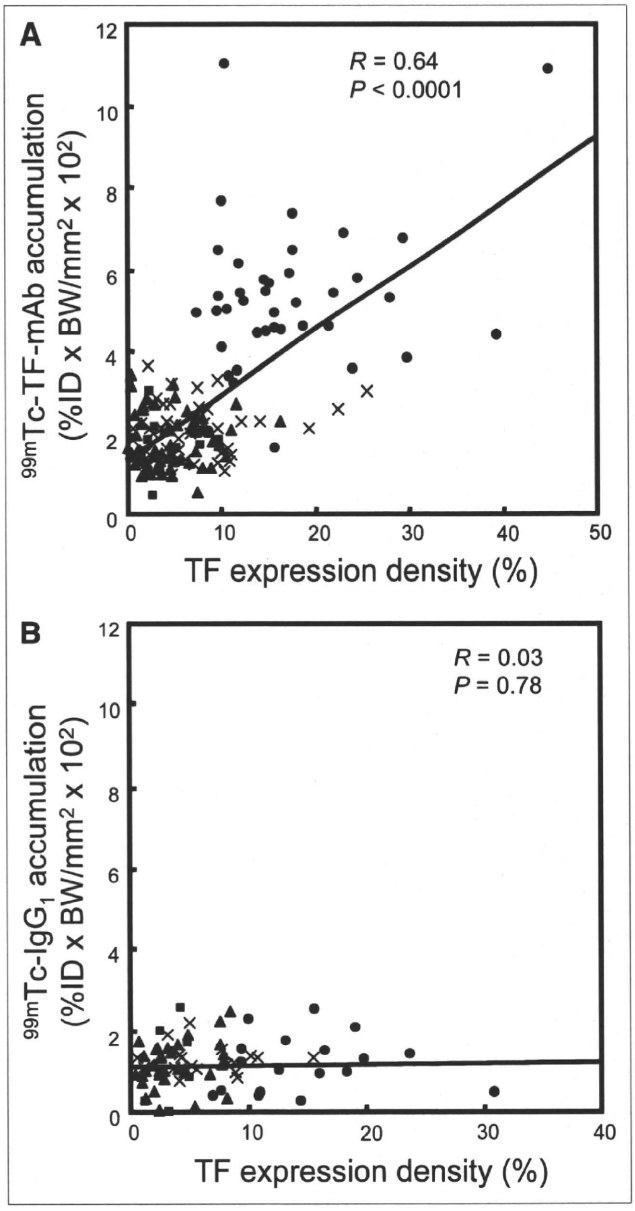

FIGURE 3. Regression analyses of TF expression density with ^{99m}Tc-TF-mAb (A) and ^{99m}Tc-IgG_1 (B) accumulation. ■ = neointimal lesion; ● = atheromatous lesion; × = fibroatheromatous lesion; ▲ = collagen-rich lesion.

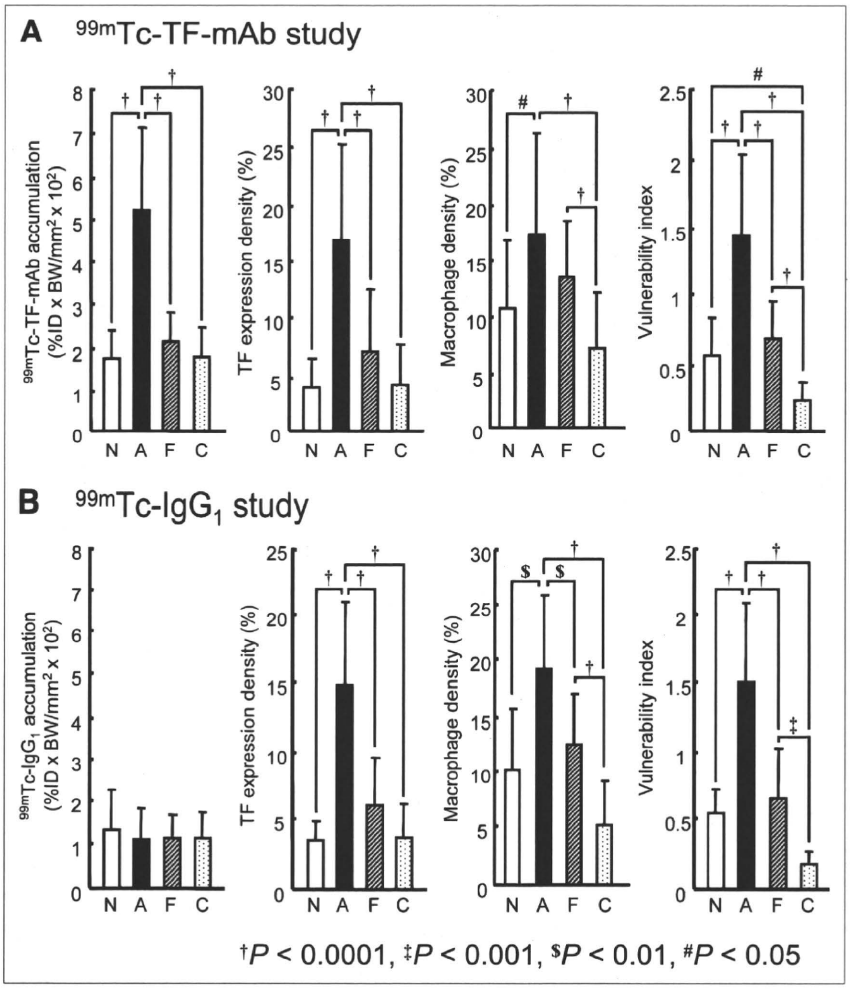

FIGURE 4. Distribution profiles of radioactivity accumulation, TF expression, macrophage density, and vulnerability index in atherosclerotic lesions in ^{99m}Tc-TF-mAb (A) and ^{99m}Tc-IgG$_1$ (B) study. A = atheromatous lesions; C = collagen-rich lesions; F = fibroatheromatous lesions; N = neointimal lesions. Data are represented as mean ± SD.

Relatively high radioactivity accumulations were found in the liver and kidneys of all 3 groups (Fig. 2). We observed that the ^{99m}Tc-TF-mAb cleared rather more slowly from the bodies of WHHLMI rabbits than from control rabbits.

Regional Distribution of ^{99m}Tc-TF-mAb, in Comparison with TF Expression

In the autoradiography study, heterogeneous ^{99m}Tc-TF-mAb accumulation was observed in the intima of WHHLMI rabbit aortas (Fig. 5B), whereas no marked accumulation was found in the aortas of control rabbits (Fig. 5A). Variable TF expression was detected in the intimal regions of the WHHLMI rabbit aorta (Figs. 5D, 5F, and 5G). Higher accumulation levels of ^{99m}Tc-TF-mAb were found in regions with high TF expression, whereas lower accumulation was observed in regions with low TF expression (Fig. 5, compare 5B with 5F and 5G). Consequently, regional ^{99m}Tc-TF-mAb accumulation levels in the aorta section were positively correlated with TF expression density in WHHLMI rabbits ($R = 0.64$, $P < 0.0001$) (Fig. 3A). No obvious TF expression was observed in the aorta of control rabbits (Figs. 5C, 5E, and 3B).

Relationship Between ^{99m}Tc-TF-mAb Accumulation and Histologic Characteristics

The plaques were categorized according to histopathologic classification criteria as follows: neointimal ($n = 12$ for ^{99m}Tc-TF-mAb study and $n = 7$ for ^{99m}Tc-IgG$_1$ study), atheromatous ($n = 40$ for ^{99m}Tc-TF-mAb study and $n = 20$ for ^{99m}Tc-IgG$_1$ study), fibroatheromatous ($n = 43$ for ^{99m}Tc-TF-mAb study and $n = 21$ for ^{99m}Tc-IgG$_1$ study), and collagen-rich ($n = 62$ for ^{99m}Tc-TF-mAb study and $n = 36$ for ^{99m}Tc-IgG$_1$ study). No lesions showed hemorrhage, plaque rupture, or thrombi (type VI). The level of ^{99m}Tc-TF-mAb accumulation was dependent on the histologic grade of the lesions (Fig. 4A) and was prominently and significantly the highest ($P < 0.0001$) in atheromatous lesions (type IV), compared with other lesions. The accumulation level of ^{99m}Tc-TF-mAb was 3.0-, 2.4-, and 2.9-fold higher in atheromatous lesions than in neointimal, fibroatheromatous, and collagen-rich lesions, respectively. The vulnerability index was also the highest in atheromatous lesions, followed in decreasing order by fibroatheromatous, neointimal, and collagen-rich lesions. Consequently, the highest level of ^{99m}Tc-TF-mAb accumulation and the highest vulnerability

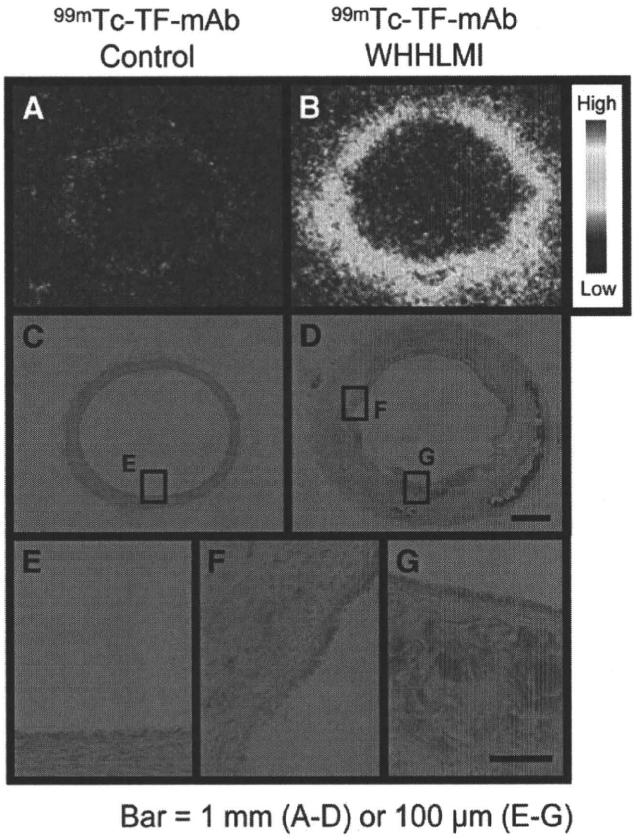

FIGURE 5. Regional distribution of ^{99m}Tc-TF-mAb and TF expression in aortic sections. Autoradiogram (A and B) and TF immunohistochemical staining (C–G) of control (C and E) and WHHLMI rabbits (D, F, and G). (E–G) High-magnification images of TF immunohistochemical staining in regions depicted in C and D. Identical color window was applied to both autoradiographic images (A and B). Bar = 1 mm (A–D) and 100 μm (E–G).

index were both observed in atheromatous lesions. In contrast, ^{99m}Tc-IgG$_1$ accumulation in lesions was low and did not correlate with the histologic grade of lesions, with no significant differences among the lesion types (Fig. 4B).

DISCUSSION

In the present study, we designed a new imaging agent, ^{99m}Tc-TF-mAb, for the purpose of discriminating atherosclerotic lesions at higher risk for rupture (thrombogenic atheromatous lesions) from more stable lesions and evaluated the potential of ^{99m}Tc-TF-mAb using an atherosclerotic rabbit model. Our major findings are that a positive correlation was demonstrated between regional ^{99m}Tc-TF-mAb accumulation and TF expression density in atherosclerotic lesions of WHHLMI rabbits but not with ^{99m}Tc-IgG$_1$ and that significantly higher ^{99m}Tc-TF-mAb accumulation was found in grade IV, more vulnerable atheromatous lesions, than in neointimal lesions or other more stable lesions. Thus, we demonstrate the potential of ^{99m}Tc-TF-mAb for molecular imaging of TF expression and selectively detecting atheromatous plaques at higher risk for rupture.

Immunoreactivity and Specificity of ^{99m}Tc-TF-mAb

Immunoreactivity, specificity, and detectable but functionally silent labeling are indispensable prerequisites of in vivo molecular imaging probes using immunodetection. In this study, flow cytometric analyses indicated that modification of TF-mAb with HYNIC did not significantly affect the immunoreactivity of the original TF-mAb. In addition, autoradiography and immunohistochemical studies showed that ^{99m}Tc-TF-mAb accumulation in atherosclerotic lesions correlated well with TF expression density, which was higher in atheromatous lesions, as expected (Figs. 3A and 4A). Further, contrary to the results with ^{99m}Tc-TF-mAb (Fig. 4A), the results with ^{99m}Tc-IgG$_1$ (Fig. 4B) showed that accumulation of ^{99m}Tc-labeled nonspecific IgG in atheromatous lesions was not significantly different from that in other types of lesions (i.e., neointimal, fibroatheromatous, and collagen-rich lesions). These findings strongly suggest the potential of ^{99m}Tc-TF-mAb to specifically recognize TF in vivo.

TF as a Target Molecule for Plaque Imaging

TF, selected as a target molecule for molecular imaging in this study, initiates the exogenous blood coagulation cascade leading to thrombus formation in vivo and represents a good marker for late-stage vulnerable lesions. TF in atherosclerotic lesions was identified in several cell types, such as endothelial cells, smooth muscle cells, monocytes, macrophages, and foam cells (*3*), similar to lectinlike oxidized low-density lipoprotein receptor 1 (LOX-1). TF expression is reported to be increased in the later stages of atheromatous progression and thus was selectively detected in atheromatous lesions in this report (Fig. 4). These findings are comparable to those of our previous immunohistochemical study (*5*) and another human study (*4*). On these bases, TF should be a potential target for detecting atheromatous plaques at higher risk for rupture in vivo. To our knowledge, this is the first report of the development of an in vivo TF imaging probe.

On the other hand, a series of imaging agents has targeted fibrin and factor XIII in thrombi using antibodies or peptides (*1*), with at least partial success. In the blood-coagulation cascade, TF initiates the system, and factor XIII covalently cross-links fibrin polymers and renders the thrombus more resistant to lysis. Therefore, ^{99m}Tc-TF-mAb will be useful for the early detection of the cascade, and fibrin and factor XIII imaging probes can detect later stages and thrombi themselves. In this study, ^{99m}Tc-TF-mAb corresponded with TF expression and showed preferential accumulation in atheromatous lesions and in lesions with increased vulnerability. Although further studies are required to investigate which target molecules in the cascade are most appropriate to estimate how unstable or vulnerable a plaque is in vivo, TF is a potential target. Furthermore, because great efforts have been made in the development of anticoagulation and antiplatelet pharmaceuticals for the treatment of atherosclerosis and

hyperlipidemia, effective imaging probes to target blood-coagulation cascades are also required for efficient drug development.

Limitations of ^{99m}Tc-TF-mAb

One drawback of ^{99m}Tc-TF-mAb is its relatively slow clearance from the blood, which is an intrinsic problem of molecular probes using antibodies. Recent advances in antibody engineering, however, should provide a promising solution for this issue. Radioprobes derived from low-molecular-weight polypeptides or compounds, small recombinant antibody fragments (Fab, scFv), engineered variants (diabodies, triabodies, minibodies, and single-domain antibodies), or pretargeting antibody methods show rapid clearance of radioactivity from the circulation (*19–21*). Image-subtraction techniques (*22–24*) or kinetic model analysis (*25,26*) may also help solve this issue. Accordingly, ^{99m}Tc-TF-mAb or its derivatives have great potential as in vivo molecular imaging probes and deserve further investigation.

A higher renal accumulation of ^{99m}Tc-IgG$_1$ than of ^{99m}Tc-TF-mAb was observed in WHHLMI rabbits. Although an exact mechanistic explanation for this significant difference is not clear, several other investigators have also reported a relatively high renal accumulation after the injection of radiolabeled mAbs (*27–29*). Because we evaluated the biodistribution 24 h after the injection (relatively late phase), renal accumulation may be ascribed to metabolic or degradation products of ^{99m}Tc-labeled antibodies (*30*). Thus, further ex vivo metabolite analysis studies could help to clarify the mechanism. In addition, it is known that the excretion system of WHHLMI rabbits is compromised (*31*), which could alter the renal accumulation of tracers. On the other hand, although a certain degree of TF expression was observed in glomeruli (*32*), this could not be a reason for the higher renal accumulation of ^{99m}Tc-IgG$_1$.

Recently, the focus of anticoagulant research has turned to inhibition of the TF-FVIIa complex, and many pharmaceutical industry research programs have attempted to discover TF-FVIIa complex inhibitors (*33*). Studies in monkeys have indicated that inhibition of the TF-FVIIa complex, compared with other anticoagulants that inhibit thrombin or FXa, results in an improved profile . It is well known that the pathways for blood coagulation are interdependent, and the initiation, amplification, and propagation stages are closely regulated by positive and negative feedback loops. Thus, repeated doses of anticoagulants might increase the expression of ineffective (silent) TF complex in plaques because of such feedback processes independent of the antiatherosclerotic effect, although a lowering of net TF expression would be expected. The TF antibody we established in this study recognizes 193Ser-207Cys in the extracellular domain, which is distant from the protein sites related to complex formation with FVIIa. Therefore, the ^{99m}Tc-TF-mAb we developed can estimate the net TF expression in plaques, providing a useful tool to investigate the effect of such anticoagulants in vivo.

Comparison with Other Imaging Probes

In the search for suitable molecular probes to assess atherosclerotic lesion characteristics, many targets, including macrophage activity, angiogenesis, apoptosis, and cell tracking (monocyte, stem cell, lymphocyte), have been assessed (*1,2,34–36*). However, the usefulness of these probes is still under preliminary investigation, except for ^{18}F-FDG, a marker of inflammation, and ^{99m}Tc-annexin A5, a marker of ongoing apoptotic cell death, which are currently in clinical studies. In previous studies, we evaluated macrophage imaging using ^{18}F-FDG (*11*) and also ^{99m}Tc-LOX-1-mAb (*17*), which targets a scavenger receptor highly expressed on macrophages and foam cells and showed the usefulness for detection of atherosclerotic lesions. However, ^{18}F-FDG accumulated in relatively stable lesions because of the presence of macrophages in such lesions, as also seen in this report (Fig. 4). We also previously showed a certain degree of LOX-1 expression in relatively stable lesions with ^{99m}Tc-LOX-1-mAb. As for ^{99m}Tc-annexin A5, the accumulation ratios of atheromatous lesions to other lesions of ^{99m}Tc-TF-mAb (atheromatous to neointimal, 3.0; atheromatous to fibroatheromatous, 2.4; and atheromatous to collagen-rich, 2.9) were markedly higher than those of ^{99m}Tc-annexin A5 (atheromatous to neointimal,1.3; atheromatous to fibroatheromatous, 1.3; atheromatous to collagen-rich, 1.8) (*15*). Our previous study in apolipoprotein E–null mice also showed relatively high ^{18}F-FDG accumulation levels in early lesions, resulting in lower accumulation ratios for advanced to early lesions in comparison with ^{99m}Tc-annexin A5 (*37*). Thus, the desirable features of ^{99m}Tc-TF-mAb further confirm its potential as a molecular probe for detecting atheromatous lesions at higher risk for rupture.

CONCLUSION

In this study, we succeeded in determining TF expression using ^{99m}Tc-TF-mAb in WHHLMI rabbits. Consequently, we demonstrated prominently higher accumulation of ^{99m}Tc-TF-mAb in grade IV atheroma. These findings strongly indicate that molecular imaging of TF should provide clinically useful information on the thrombogenicity of atherosclerotic plaques.

ACKNOWLEDGMENTS

This work was partly supported by a grant-in-aid for general scientific research from the Ministry of Education, Culture, Sports, Science and Technology of Japan and from the Japan Society for the Promotion of Science and by a research grant from the Association for Nuclear Technology in Medicine and Takeda Science Foundation.

REFERENCES

1. Shaw SY. Molecular imaging in cardiovascular disease: targets and opportunities. *Nat Rev Cardiol.* 2009;6:569–579.
2. Saraste A, Nekolla SG, Schwaiger M. Cardiovascular molecular imaging: an overview. *Cardiovasc Res.* 2009;83:643–652.

3. Moons AH, Levi M, Peters RJ. Tissue factor and coronary artery disease. *Cardiovasc Res.* 2002;53:313–325.
4. Jeanpierre E, Le Tourneau T, Six I, et al. Dietary lipid lowering modifies plaque phenotype in rabbit atheroma after angioplasty: a potential role of tissue factor. *Circulation.* 2003;108:1740–1745.
5. Kuge Y, Kume N, Ishino S, et al. Prominent lectin-like oxidized low density lipoprotein (LDL) receptor-1 (LOX-1) expression in atherosclerotic lesions is associated with tissue factor expression and apoptosis in hypercholesterolemic rabbits. *Biol Pharm Bull.* 2008;31:1475–1482.
6. Shiomi M, Ito T, Yamada S, Kawashima S, Fan J. Development of an animal model for spontaneous myocardial infarction (WHHLMI rabbit). *Arterioscler Thromb Vasc Biol.* 2003;23:1239–1244.
7. Abrams MJ, Juweid M, tenKate CI, et al. Technetium-99m-human polyclonal IgG radiolabeled via the hydrazino nicotinamide derivative for imaging focal sites of infection in rats. *J Nucl Med.* 1990;31:2022–2028.
8. Ono M, Arano Y, Mukai T, et al. Plasma protein binding of ^{99m}Tc-labeled hydrazino nicotinamide derivatized polypeptides and peptides. *Nucl Med Biol.* 2001;28:155–164.
9. Larsen SK, Solomon HF, Caldwell G, Abrams MJ. [^{99m}Tc]tricine: a useful precursor complex for the radiolabeling of hydrazinonicotinate protein conjugates. *Bioconjug Chem.* 1995;6:635–638.
10. Ishii K, Kita T, Kume N, Nagano Y, Kawai C. Uptake of acetylated LDL by peritoneal macrophages obtained from normal and Watanabe heritable hyperlipidemic rabbits, an animal model for familial hypercholesterolemia. *Biochim Biophys Acta.* 1988;962:387–389.
11. Ogawa M, Ishino S, Mukai T, et al. ^{18}F-FDG accumulation in atherosclerotic plaques: immunohistochemical and PET imaging study. *J Nucl Med.* 2004;45:1245–1250.
12. Stary HC, Chandler AB, Glagov S, et al. A definition of initial, fatty streak, and intermediate lesions of atherosclerosis: a report from the Committee on Vascular Lesions of the Council on Arteriosclerosis, American Heart Association. *Circulation.* 1994;89:2462–2478.
13. Stary HC, Chandler AB, Dinsmore RE, et al. A definition of advanced types of atherosclerotic lesions and a histological classification of atherosclerosis: a report from the Committee on Vascular Lesions of the Council on Arteriosclerosis, American Heart Association. *Circulation.* 1995;92:1355–1374.
14. Kobayashi S, Inoue N, Ohashi Y, et al. Interaction of oxidative stress and inflammatory response in coronary plaque instability: important role of C-reactive protein. *Arterioscler Thromb Vasc Biol.* 2003;23:1398–1404.
15. Ishino S, Kuge Y, Takai N, et al. ^{99m}Tc-Annexin A5 for noninvasive characterization of atherosclerotic lesions: imaging and histological studies in myocardial infarction-prone Watanabe heritable hyperlipidemic rabbits. *Eur J Nucl Med Mol Imaging.* 2007;34:889–899.
16. Shiomi M, Ito T, Hirouchi Y, Enomoto M. Stability of atheromatous plaque affected by lesional composition: study of WHHL rabbits treated with statins. *Ann N Y Acad Sci.* 2001;947:419–423.
17. Ishino S, Mukai T, Kuge Y, et al. Targeting of lectinlike oxidized low-density lipoprotein receptor 1 (LOX-1) with ^{99m}Tc-labeled anti-LOX-1 antibody: potential agent for imaging of vulnerable plaque. *J Nucl Med.* 2008;49:1677–1685.
18. Shiomi M, Ito T, Hirouchi Y, Enomoto M. Fibromuscular cap composition is important for the stability of established atherosclerotic plaques in mature WHHL rabbits treated with statins. *Atherosclerosis.* 2001;157:75–84.
19. Huhalov A, Chester KA. Engineered single chain antibody fragments for radioimmunotherapy. *Q J Nucl Med Mol Imaging.* 2004;48:279–288.
20. Sharkey RM, Karacay H, Cardillo TM, et al. Improving the delivery of radionuclides for imaging and therapy of cancer using pretargeting methods. *Clin Cancer Res.* 2005;11:7109s–7121s.
21. Sano K, Temma T, Kuge Y, et al. Radioimmunodetection of membrane type-1 matrix metalloproteinase relevant to tumor malignancy with a pre-targeting method. *Biol Pharm Bull.* 2010;33:1589–1595.
22. Temma T, Iida H, Hayashi T, et al. Quantification of regional myocardial oxygen metabolism in normal pigs using positron emission tomography with injectable ^{15}O-O_2. *Eur J Nucl Med Mol Imaging.* 2010:37:377–385.
23. Yamamoto Y, de Silva R, Rhodes CG, et al. Noninvasive quantification of regional myocardial metabolic rate of oxygen by $^{15}O_2$ inhalation and positron emission tomography: experimental validation. *Circulation.* 1996;94:808–816.
24. Iida H, Rhodes CG, Araujo LI, et al. Noninvasive quantification of regional myocardial metabolic rate for oxygen by use of $^{15}O_2$ inhalation and positron emission tomography: theory, error analysis, and application in humans. *Circulation.* 1996;94:792–807.
25. Watabe H, Ikoma Y, Kimura Y, Naganawa M, Shidahara M. PET kinetic analysis: compartmental model. *Ann Nucl Med.* 2006;20:583–588.
26. Ikoma Y, Watabe H, Shidahara M, Naganawa M, Kimura Y. PET kinetic analysis: error consideration of quantitative analysis in dynamic studies. *Ann Nucl Med.* 2008;22:1–11.
27. Rogers BE, Anderson CJ, Connett JM, et al. Comparison of four bifunctional chelates for radiolabeling monoclonal antibodies with copper radioisotopes: biodistribution and metabolism. *Bioconjug Chem.* 1996;7:511–522.
28. Sugimoto K, Nishimoto N, Kishimoto T, Yoshizaki K, Nishimura T. Imaging of lesions in a murine rheumatoid arthritis model with a humanized anti-interleukin-6 receptor antibody. *Ann Nucl Med.* 2005;19:261–266.
29. D'Alessandria C, Malviya G, Viscido A, et al. Use of a ^{99m}Tc labeled anti-TNFα monoclonal antibody in Crohn's disease: in vitro and in vivo studies. *Q J Nucl Med Mol Imaging.* 2007;51:334–342.
30. Akizawa H, Arano Y. Altering pharmacokinetics of radiolabeled antibodies by the interposition of metabolizable linkages: metabolizable linkers and pharmacokinetics of monoclonal antibodies. *Q J Nucl Med.* 2002;46:206–223.
31. Campean V, Neureiter D, Varga I, et al. Atherosclerosis and vascular calcification in chronic renal failure. *Kidney Blood Press Res.* 2005;28:280–289.
32. Drake TA, Morrissey JH, Edgington TS. Selective cellular expression of tissue factor in human tissues: implications for disorders of hemostasis and thrombosis. *Am J Pathol.* 1989;134:1087–1097.
33. Prezelj A, Anderluh PS, Peternel L, Urleb U. Recent advances in serine protease inhibitors as anticoagulant agents. *Curr Pharm Des.* 2007;13:287–312.
34. Davies JR, Rudd JH, Weissberg PL, Narula J. Radionuclide imaging for the detection of inflammation in vulnerable plaques. *J Am Coll Cardiol.* 2006;47(8, suppl):C57–C68.
35. Jaffer FA, Libby P, Weissleder R. Molecular and cellular imaging of atherosclerosis: emerging applications. *J Am Coll Cardiol.* 2006;47:1328–1338.
36. Rudd JH, Hyafil F, Fayad ZA. Inflammation imaging in atherosclerosis. *Arterioscler Thromb Vasc Biol.* 2009;29:1009–1016.
37. Zhao Y, Kuge Y, Zhao S, et al. Comparison of ^{99m}Tc-annexin A5 with ^{18}F-FDG for the detection of atherosclerosis in ApoE−/− mice. *Eur J Nucl Med Mol Imaging.* 2007;34:1747–1755.

Erratum

In the article "^{18}F-FDG PET After 2 Cycles of ABVD Predicts Event-Free Survival in Early and Advanced Hodgkin Lymphoma," by Cerci et al. (*J Nucl Med.* 2010;51:1337–1343), Figure 4 contained a mistake. The graph of event-free survival in patients with a low International Prognostic Score should indicate that 10 of 18 patients (not 3 of 30) were PET2-positive. The authors regret the error.

特集　トランスレーショナルリサーチに貢献するウサギ

高コレステロール血症，心血管疾患に関するトランスレーショナルリサーチにおけるWHHLMIウサギの有用性

塩見　雅志，伊藤　隆
神戸大学 大学院 医学研究科 附属動物実験施設

1．はじめに

WHOの調査によると，WHO加盟国の死因の第一位は心血管疾患であり，死因の約30%を占めている。わが国では，死因の第一位は悪性新生物（がん），第2位が心血管疾患であり，心血管疾患はわが国においても克服しなければならない重要な疾患である。心血管疾患の危険因子として，高コレステロール血症，高血圧，糖代謝異常，喫煙，加齢，男性などが指摘されている。なかでも，血清脂質値の管理が重要とされており，現在の日本人の正常値は，血清総コレステロールの上限が220mg/dl，動脈硬化の原因になると考えられているLDL（低比重リポ蛋白）コレステロールの上限が140mg/dl，動脈硬化抑制因子であるHDL（高比重リポ蛋白）コレステロールの下限が40mg/dlとされている。1980年代以降の研究により，血清総コレステロール値と心血管疾患の発生率の間に高い相関があり，薬剤等で血清総コレステロール値を低下させると心血管疾患の発生を抑制できることが示された。コレステロール低下剤の開発は，日本の製薬会社（旧三共株式会社）が世界に先駆けて開発したコレステロール合成阻害剤（HMG-CoA還元酵素阻害剤，通称スタチン）が契機となり，その薬効評価に使用された実験動物が，故渡辺嘉雄先生（神戸大学）が開発されたWHHL（Watanabe heritable hyperlipidemic）ウサギであった[1]。旧三共株式会社の研究スタッフは，当初ラットを用いて薬効評価を実施したが，コレステロール低下作用は認められず開発を断念しかけていた。しかし，培養系とニワトリでの強いコレステロール合成阻害作用から，このスタチンの薬効を評価できる哺乳動物の探索を行なっていた。彼らによって麻布大学の紀要に掲載されていたWHHLウサギが見出され，WHHLウサギがスタチンの開発に貢献することになった。それは1979年のことであった。現在市場に出ているスタチンは7種類以上あり，世界中で2,000万人以上に処方される薬剤に成長し，スタチンの服用で心血管疾患による死亡率が対象群に比較して20～50%低下すると報告され，高脂血症や心血管疾患の治療に欠かせない薬剤となった。この経緯は，薬剤の開発というトランスレーショナルリサーチを遂行するに当たり，適切な動物種を選定することがいかに重要であるかを如実に物語っている。本総説では，WHHLMIウサギの開発過程とスタチンの開発におけるWHHLウサギのかかわりをとおして，トランスレーショナルリサーチにおける動物種選定の重要性を考えてみたい。

2．WHHLウサギ開発の歴史と特性

WHHLウサギは1973年に偶然発見された高脂血症を示す1匹のオスの日本白色種ウサギに由来する。8年間の交配実験を通して系統として確立された。当初，HLR（Hyperlipidemic rabbit）と命名され，その後開発者の名前を付すべきとの助言により，WHL（Watanabe-hyperlipidemic）ウサギと改名された。その後，動脈硬化の国際誌に投稿した際に編集者の一人からの助言で，WHHLウサギと命名された[2]。

系統として確立した当時のWHHLウサギは，成熟齢における血清総コレステロール値が300～700mg/dl，中性脂肪値が300～400mg/dlであり，大動脈に動脈硬化が発生し，四肢の指関節に黄色腫が発生した[1]。血圧，血糖値等は正常レベルであった。スタチンの開発に当たり，旧三共株式会社の研究スタッフはWHHLウサギの高脂血症の発症機序の解明を試みた。その結果，細胞表面に発現するLDL受容体の活性が顕著に低下し，血中からのLDLの異化が遅延し，血中にLDLが蓄積していることが明らかにされた[2,3]。これらの所見は，ヒトの家族性高コレステロール血症（FH）にきわめて類似しており，世界初のFHの自然発症のモデル動物であることが確認された。その後，1985年にノーベル賞を受賞したGoldstein JLとBrown MSの研究グループが，彼らが提唱していたリポ蛋白代謝におけるLDL受容体仮説をWHHLウサギを用いて証明した。彼らの研究によってヒトのリポ蛋白代謝が解明され，WHHLウサギのリポ蛋白代謝はヒトのリポ蛋白代謝に類似していることが明らかとなった。WHHLウサギ血中のリポ蛋白の組成および代謝がヒトに類似していたことから，WHHLウサギはコレステロール低下剤の開発研究に広く使用されるようになった。

高脂血症のモデル動物として重要なことは，ヒトの高脂血症で最後のイベントとなる心筋梗塞が発症することである。心筋梗塞の発症には心臓の冠動脈に動脈硬化が発生することが必須条件であるが，系統として確立した当時のWHHLウサギでは冠動脈の動脈硬化発生率はきわめて低値であった。神戸大学では冠動脈に動脈硬化が発生するWHHLウサギを開発するべく，選抜交配を実施し，1985年に冠動脈疾患を好発するWHHLウサギを開発し，1992年には重度の冠動脈病変が発生するWHHLウサギを開発した。しかし，心筋梗塞の発生率は改善されず低率であった。その後7年間の選抜交配の結果，動脈硬化による冠動脈の閉塞によって心筋梗塞が発生するWHHLMIウサギの開発に成功した[4]。これらの系統開発の過程で，大動脈と冠動脈の動脈硬化病変には質的に違いがあることが示唆され，冠動脈病変に対する薬剤の抑制効果を確認できる数少ない実験動物となった。しかし，WHHLウサギは開発過程によって冠動脈病変の発生状況が異なるため，どのステージのWHHLウサギであるかを確認する必要がある。なお，冠動脈に動脈硬化が安定して発生するWHHLウサギはWHHLMIウサギである。

これらの系統開発過程において，動脈硬化の発生機序の解明にWHHLウサギが用いられ，動脈硬化病変に酸化LDLが蓄積していること，LDLの酸化を抑制すると動脈硬化の発生・進展を抑制できること，動脈硬化が発生する際には動脈内皮にリンパ球接着因子が発現し，単球が接着して内皮下に侵入し，マクロファージとなって酸化LDLを貪食し，動脈硬化病変が形成されること等が解明された[2,3]。

3．脂質代謝，動脈硬化における種差

ウサギのリポ蛋白代謝はヒトに類似していることを上述した。リポ蛋白代謝がヒトと大きく異なれば，その動物種は脂質低下剤を開発する上で大きな障害となる。実験動物の代表であるマウスや

表1　ヒトの脂質代謝，動脈硬化，心機能解析等に対する高脂血症の遺伝子組換えマウスとウサギの類似性

	遺伝子組換 マウス*	WHHLMI ウサギ
脂質代謝		
血中の主要リポ蛋白	×（カイロミクロン，VLDL）	○（LDL）
内因性リポ蛋白の構造蛋白	×（apoB48）	○（apoB100）
アポB編集酵素の発現	×（小腸，肝）	○（小腸）
血中CETP活性	×（無）	○（有）
肝性リパーゼ	×（遊離）	○（血管壁に結合）
動脈硬化		
冠動脈	×（抵抗性）	△（自然発症）
病変の構成	×（脂質過剰蓄積）	○（種々の病変）
心臓		
心電図　四肢誘導	×（大きく異なる）	○（ヒトに類似）
胸部誘導	×（モニター困難）	○（ヒトに類似）
その他		
炎症マーカー	×（SAP）	○（CRP）
脂質低下剤**の効果	×（抵抗性）	○（有）

*apoE（−/−）マウス，LDLR（−/−）マウス
**スタチン（HMG-CoA還元酵素阻害剤，コレステロール合成阻害剤）

ラットでは脂質代謝がヒトと大きく異なる（表1）。マウス・ラットのリポ蛋白代謝でヒトやウサギと大きく異なる点は複数ある[2,3]。主な点は次のとおりである。1）apoB編集酵素が肝臓で発現する。その結果，ヒトやウサギの内因性リポ蛋白は構造蛋白としてapoB-100を有するが，マウスやラットでは外因性リポ蛋白と同じapoB-48を有する。apoB-48を持つリポ蛋白の代謝回転はきわめて速く，マウスやラットでは血中におけるリポ蛋白の構成がヒトと大きく異なる一因となっている。2）肝性リパーゼが血中に遊離している。その結果，中性脂肪の分解と遊離脂肪酸の組織への受け渡しがヒトと異なる。3）コレステロールエステル転送蛋白が発現していない。その結果，末梢組織から回収されたコレステロールがLDL等に渡されず，血中のHDLコレステロールの比率が増大し，血中のリポ蛋白の構成がヒトと大きく異なる。4）コレステロール合成の律速酵素の活性が強い。その結果コレステロール合成阻害剤に対して抵抗性を示す。したがって，マウスやラットの高脂血症のモデルでは血中に鬱滞しているリポ蛋白の種類がヒトと異なり，脂質低下剤の開発の障害になっている。また，ヒトの炎症マーカーであるC-反応性蛋白（CRP）はマウスやラットでは機能しておらず，動脈内皮細胞の機能にも差異が認められ，心筋線維の種類もヒトやウサギと異なることが知られている。さらに心電図所見もマウスやラットはヒトと大きく異なるがウサギはヒトに類似している。このようにマウスやラットでは脂質代謝や心血管疾患に関連する因子がヒトやウサギと大きく異なっている。したがって，マウスやラットをこれらの分野の実験に使用する場合には十分な配慮が必要となるであろう。

4．脂質低下剤の開発におけるトランスレーショナルリサーチ

WHHLウサギはリポ蛋白代謝がヒトにきわめて類似していることから，さまざまな脂質低下剤の開発に用いられてきた（表2）[2,3]。コレステロール合成阻害剤（コレステロール合成の上流に位置す

表2 WHHL／WHHLMIウサギを用いた薬剤開発研究

	脂質低下効果	動脈硬化抑制効果 大動脈	冠動脈
コレステロール合成阻害剤			
スタチン	○	×, ○	○
スクアレン合成阻害剤	○	○	○
陰イオン交換樹脂剤	○	○	
スタチン＋インイオン交換樹脂剤	○	○	○
MTP阻害剤	○		
ACAT阻害剤	×, ○	×, ○	×, ○
抗酸化剤			
プロブコール	○	○	
ビタミンE	×	×, ○	
コロニー刺激因子			
MCSF	×, ○	○	
GMCSF	×, ○	○	
アポE	×, ○	○	
フィブラート	×		
魚油，ω3脂肪酸	×, ○	×, ○	
チアゾリディンディオン	×	△	△
チアゾリディンディオン+スタチン	○	○	○
ACE阻害剤	×	○	
A-II受容体拮抗剤	×	○	
カルシウム拮抗剤	×	×	
βブロッカー	×	×	
遺伝子治療	○		

るHMG-CoA還元酵素や下流に位置するスクアレン合成酵素などの阻害剤），魚油等で代表されるω－3系脂肪酸，胆汁酸を吸着して腸－肝循環を遮断する陰イオン交換樹脂製剤，中性脂肪の低下作用を持つフィブラート系薬剤などの薬効が調べられ，コレステロール合成阻害剤と陰イオン交換樹脂製剤でコレステロール低下効果が確認されている。コレステロール合成阻害剤の一つであるスタチンを用いた研究では，投与用量に依存して血清総コレステロールが低下（対照群に比較して10～30％低下）した。コレステロール低下のメカニズムは，肝臓でのコレステロール合成抑制に伴うLDL受容体の増加による血中LDLの低下と，高用量の場合の肝からのVLDL（超低比重リポ蛋白）コレステロールの分泌低下の二つのメカニズムが関与していることが示唆された。スクアレン合成阻害剤も同様の作用機序で血清コレステロール値を低下させると考えられる。WHHLウサギはLDL受容体異常のdefective typeであることから，肝細胞におけるコレステロール合成阻害によって細胞表面に到達するLDL受容体蛋白が増加することが推測できる。陰イオン交換樹脂製剤は十二指腸で胆汁酸を吸着し腸－肝循環を遮断する。その結果，肝においてコレステロールが胆汁酸の材料として消費され，肝細胞がコレステロール不足となってLDL受容体が増加することが示されている。したがって，コレステロール合成阻害剤と陰イオン交換樹脂製剤の併用投与によって血清総コレステロール値は相加的に減少することもWHHLウサギを用いた研究で示されている。このことは，一般的

な高コレステロール血症に加えて，LDL受容体に異常があるヒトの家族性高コレステロール血症（除くLDL受容体ネガティブタイプ）においても，薬物治療が可能であることを示唆している。

5．脂質低下剤の動脈硬化抑制作用に関するトランスレーショナルリサーチ

血清総コレステロール値を低下させる目的は，動脈硬化を抑制し，心血管イベントや脳血管イベントを抑制することにある。コレステロール低下剤の投与によって動脈硬化が抑制できることがWHHLウサギを用いた研究で初めて証明された（表2）。スタチンを高用量で8ヵ月投与すると，血清総コレステロール値が20～30％低下し，冠動脈の狭窄率が対照群に比較して有意に低下した[5]。しかし，臨床における冠動脈造影による評価で，スタチンの投与で冠動脈狭窄率の改善が認められないケースにおいても心血管イベントの発生が有意に抑制できることが確認された。そのメカニズムの解明にもWHHLウサギが用いられた[6]。冠動脈にすでに動脈硬化が完成している成熟齢（10月齢）のWHHLウサギ（冠動脈病変好発系）にスタチンを1年間投与すると，冠動脈病変の進展抑制と同時に，動脈硬化病変中のマクロファージや脂質の蓄積の減少，コラーゲンなどの線維成分の増加と平滑筋細胞の減少の抑制が生じ，その結果，動脈硬化病変が破綻（病変が破れて血栓を生じる）しにくい安定な病変に質的に改善されることが明らかとなった。この研究によって，スタチンの動脈硬化病変安定化作用が心イベントの発生抑制に重要であることが確認された。スタチンの動脈硬化安定化作用が示されたことも一因となってスタチンの開発と処方される患者数は急激に増加した。また，動脈硬化の安定化が心イベントの抑制における重要な要素であることをvivoの実験で裏付けることができたことは，重要であった。コレステロール合成の下流部分を阻害するスクアレン合成阻害剤も同様の効果を示した。また，脂肪酸の質を換えて中性脂肪を低下させるω－3系脂肪酸，抗酸化剤，マクロファージの機能を調節する薬剤，アンギオテンシン系を阻害する薬剤などの動脈硬化抑制作用もWHHLウサギを用いて確認された[2,3]。このようにWHHLウサギは動脈硬化抑制作用に関する研究にきわめて有効である。

6．動脈硬化のイメージング

動脈硬化の進展を抑制あるいは治療する薬剤が開発された場合に必要になるのがヒトにおける薬効評価である。冠動脈病変の程度については冠動脈造影で病変の影を見ることができるが，び漫性に病変が広く発生している場合や冠動脈が動脈硬化によるリモデリングで外側に拡大している[7]場合には，病変の程度を判定することが困難となる。さらに，動脈硬化の破綻につながる危険な病変を非観血的に調べる技術と装置の開発は，治療効果の判定のみならず心血管イベントの発生予防においてもきわめて重要である。また，心血管イベントの原因になる動脈硬化病変として，マクロファージや脂質が蓄積したソフトプラークが重要と考えられており，このソフトプラークを検出する方法として，CT（Computed Tomography，コンピュータ断層撮影），PET（Positron Emission Tomography，陽電子放射断層撮影），CT＋PET，MR（Magnetic Resonance，核磁気共鳴），IVUS（Intravascular Ultrasound，血管内超音波エコー）などを用いた方法がWHHLMIウサギを用いて研究されている[2,3]。一例として，抗酸化剤をWHHLMIウサギに投与し，その動脈硬化抑制効果がCT＋PETで確認されている[8]。さらに研究が進み，動脈硬化病変のイメージング技術が確立すると，薬剤の効果の判定のみならず，心筋梗塞などの心血管イベントの原因になる危険性を持つ冠動脈病変